Article

Immunity

HIV broadly neutralizing antibody escape dynamics drive the outcome of AAV-vectored immunotherapy in humanized mice

Graphical abstract

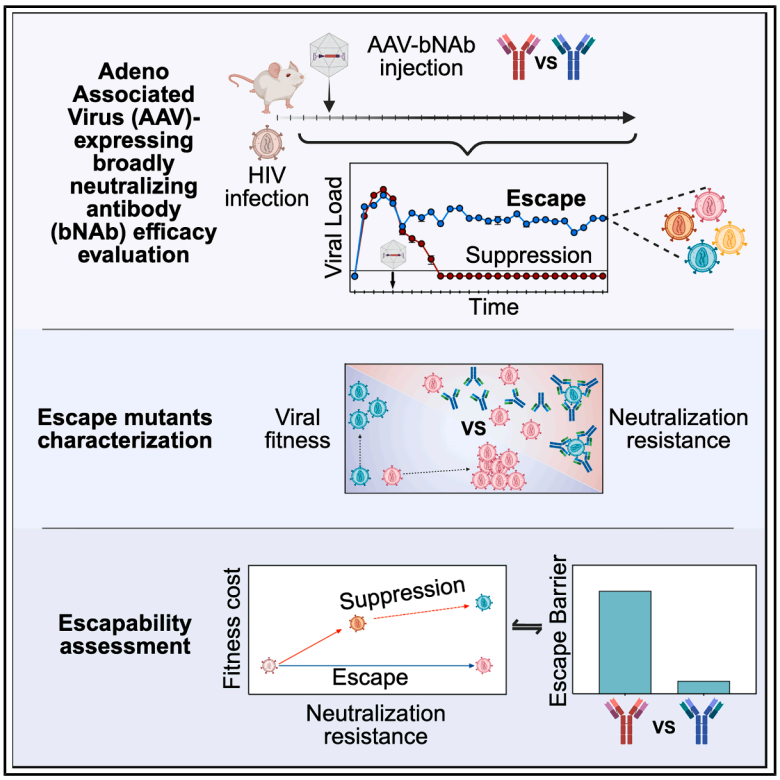

Highlights

- AAV-delivered bNAbs suppress HIV in humanized BLT mice
- Viral escape paths are conserved across virus-bNAb combinations
- Escape paths are driven by a tradeoff between fitness cost and resistance benefit
- Fitness cost and resistance benefit can be modulated to improve therapeutic efficacy

Authors

Nicolas M.S. Galvez, Adam D. Nitido, Seo Bin Yoo, ..., Vladimir D. Vrbanac, Daniel Lingwood, Alejandro B. Balazs

Correspondence

abalazs@mgh.harvard.edu

In brief

Broadly neutralizing antibodies are promising therapeutics for ending the HIV pandemic; however, their clinical efficacy is undermined by viral escape. Galvez, Nitido, et al. could drive the therapeutic outcomes of vectored immunotherapy in humanized mice by modulating the fitness costs and resistance benefits of HIV escape from AAV-vectored bNAbs.

Galvez et al., 2026, Immunity *59*, 768–782
March 10, 2026
https://doi.org/10.1016/j.immuni.2026.01.031

CellPress

CellPress

Immunity

Article

HIV broadly neutralizing antibody escape dynamics drive the outcome of AAV-vectored immunotherapy in humanized mice

Nicolas M.S. Galvez,[1,3] Adam D. Nitido,[1,3] Seo Bin Yoo,[1] Yi Cao,[1] Cailin E. Deal,[1] Christine L. Boutros,[1] Scott W. MacDonald,[1] Yentli E. Soto Albrecht,[1] Evan C. Lam,[1] Maegan L. Sheehan,[1] Dylan Parsons,[1] Allen Z. Lin,[1] Martin J. Deymier,[1] Jacqueline M. Brady,[1] Benjamin Moon,[1] Christopher B. Bullock,[1] Serah Tanno,[1] Amarendra Pegu,[2] Xuejun Chen,[2] Cuiping Liu,[2] Richard A. Koup,[2] John R. Mascola,[2] Vladimir D. Vrbanac,[1] Daniel Lingwood,[1] and Alejandro B. Balazs[1,4,*]

[1]Ragon Institute of Massachusetts General Hospital, Massachusetts Institute of Technology, and Harvard University, Cambridge, MA 02139, USA

[2]Vaccine Research Center, National Institute of Allergy and Infectious Diseases and National Institutes of Health, Bethesda, MD 20892, USA

[3]These authors contributed equally

[4]Lead contact

*Correspondence: abalazs@mgh.harvard.edu

https://doi.org/10.1016/j.immuni.2026.01.031

SUMMARY

Broadly neutralizing antibodies (bNAbs) have shown promise for the prevention and treatment of HIV. Potency and breadth measured *in vitro* are often used as predictors of clinical potential; however, human studies demonstrate that the clinical efficacy of bNAbs can be undermined by both preexisting and *de novo* resistance. Here, we found that HIV-infected humanized mice receiving bNAbs delivered via adeno-associated virus (AAV) as vectored immunotherapy (VIT) could be used to identify antibody escape paths, which were largely conserved for each bNAb. Path selection and consequent therapeutic success were driven by the fitness cost and resistance benefit of emerging mutations. Applying this framework, we independently modulated bNAb resistance or the fitness cost of escape mutants, resulting in the enhanced efficacy of VIT. This escape-path analysis successfully explains the therapeutic efficacy of bNAbs and enables a tractable means of quantifying and comparing the potential for viral escape from therapeutics *in vivo*.

INTRODUCTION

Despite substantial efforts to develop therapies and vaccines, HIV-1 remains a global pandemic. Current antiretroviral therapy (ART) regimens can effectively prevent and treat HIV infections, and emerging long-acting agents such as lenacapavir show remarkable efficacy in preventing viral acquisition.[1,2] However, their therapeutic success still requires strict adherence to the regimen, as viral rebound is swiftly observed upon treatment interruption and may lead to the development of ART resistance.[1] This is of particular relevance when access to healthcare is interrupted.[3] Over the past decade, broadly neutralizing antibodies (bNAbs) have been extensively described and characterized.[4,5] These antibodies target different sites of vulnerability on the HIV envelope (Env) protein and can prevent infection across HIV clades.[4] Their clinical success is often predicted by using metrics determined *in vitro* across large panels of diverse viral isolates.[6] These measurements consist of potency, the average inhibitory concentration needed to block 50% infection (IC_{50}) across all tested isolates, as well as breadth, the fraction of isolates neutralized at a given antibody concentration.[7] Recent advances in antibody isolation have identified new bNAbs with median potencies as low as 0.003 μg/mL[8,9] and breadth capable of neutralizing up to 96% of a panel of 208 viruses at an IC_{50} of <1 μg/mL.[10]

Given their potential, significant efforts have been made to advance bNAb-based therapies, with multiple studies demonstrating their success in preventing HIV infection in mouse[11–16] and non-human primate (NHP) models.[17–21] These findings paved the way for the antibody-mediated protection (AMP) studies (NCT02716675 and NCT02568215), two international harmonized phase 2b randomized controlled trials assessing the capacity of the CD4 binding site (CD4bs)-targeting bNAb VRC01 to prevent HIV-1 acquisition.[22] While VRC01 prevents the transmission of neutralization-sensitive strains, overall efficacy is limited by the large fraction of circulating strains with mutations conferring resistance to neutralization.[23,24] Numerous additional studies also demonstrate the potential for bNAb administration to transiently suppress HIV viremia in animal models[25–32] as well as in people living with HIV (PLWH) who harbor sensitive viruses.[33–40] However, these studies also reveal that even combinations of two or three bNAbs targeting different sites of vulnerability can fail to control viremia due to the emergence of escape mutations.[38,41,42]

The clinical translation of bNAbs is also hindered by the need for repeated infusions to maintain serum concentrations above a therapeutic threshold.[43] To overcome this, we and others have described vectored immunoprophylaxis (VIP),[12] which utilizes a single intramuscular (IM) injection of recombinant adeno-associated viral (AAV) vectors engineered to encode a bNAb transgene.[44–47] VIP induces the production of durable and protective concentrations of antibodies *in vivo*.[48] Studies of VIP with VRC07, a CD4bs-targeting bNAb clonally related to VRC01 but with greater potency and breadth,[8,17] demonstrate that delivery via AAV8 prevents intravenous and mucosal transmission of HIV in humanized mice[11,12,16] and of SIV/SHIV in NHP models.[49,50] Recently, the VRC603 trial administered AAV8-VRC07[11,51] to ART-suppressed patients (NCT03374202). In this study, up to 3 μg/mL of VRC07 is detected in serum for at least 3 years following a single IM administration.[51] Despite these promising results, anti-drug antibodies (ADAs) emerge in a subset of participants, highlighting one of the challenges of this approach. However, recent studies suggest that ADAs may be less likely to emerge in settings of increased immune tolerance, such as transient immunosuppression of adult NHPs[52] or in pediatric settings.[53]

The therapeutic potential of bNAbs delivered via AAV as vectored immunotherapy (VIT) to cure an established HIV infection is an area of active investigation, given its potential use in resource-limited settings where ART adherence is suboptimal.[53] In particular, the success of VIT can be hindered by the selection of escape variants, as seen during previous trials of passively transferred bNAbs.[54] Here, we used VIT in HIV-infected humanized mice as an experimental model to evaluate viral suppression and profile the emergence of Env mutations leading to viral escape from individual vectored antibodies. We chose two widely used clade B, tier 2 isolates for this: $HIV_{JR\text{-}CSF}$, a chronic virus cloned from the CSF of a person who died of severe AIDS encephalopathy[55]; and $HIV_{REJO.c}$, a transmitter/founder isolate that was computationally derived as the likely strain that initiated a heterosexual transmission.[56] Both of these isolates represent clinically relevant viruses, as they were cloned soon after isolation and have not been extensively cultured *in vitro*, unlike laboratory-adapted strains (e.g., $HIV_{NL4\text{-}3}$).[57] To our surprise, AAV8-VRC07 treatment drove viral evolution toward a high fitness cost escape path that often failed to emerge, enabling long-term suppression of $HIV_{REJO.c}$. Interestingly, while necessary for activity, traditional breadth and potency metrics were insufficient to predict therapeutic outcome. Instead, the specific fitness cost and resistance benefit tradeoffs of the primary escape paths best explained the success of VIT. To understand this dynamic, we adapted the fitness landscape[58] framework and created an "escapability" map for each antibody-strain combination, effectively explaining VIT outcomes by identifying the most traversed escape paths during vectored antibody therapy. Our data showed that escape pathway dynamics are a key component to understanding the *in vivo* efficacy of antibody-mediated therapies against HIV and that future therapeutic strategies that increase the fitness cost of the primary escape paths are essential for clinical success.

RESULTS

VRC07, but neither N6 nor PGDM1400, suppresses $HIV_{REJO.c}$ replication in humanized mice

To explore whether VIT could be used as a long-lived therapeutic strategy for suppressing ongoing HIV replication, we employed the bone-marrow-liver-thymus (BLT) humanized mouse model.[59–61] BLT mice were infected with $HIV_{REJO.c}$, a clade B, tier 2, CCR5-tropic, transmitted/founder infectious molecular clone (IMC) of HIV.[56] Prior to treatment, the virus was allowed to propagate and diversify in the host for 4 weeks (Figure 1A). Groups of BLT mice harboring established $HIV_{REJO.c}$ infections were given a single IM injection of 5×10^{11} genome copies (GCs) of AAV8 expressing either VRC07, N6, or PGDM1400 bNAbs or luciferase as a negative control. Importantly, all the tested bNAbs potently neutralized $HIV_{REJO.c}$ *in vitro* (Figure 1B; Table S1). After vector administration, antibody concentration in all mice increased over a period of 6 weeks (Figure 1C).

Infected mice exhibited mean plasma viral loads averaging 5.34×10^5 copies per mL of plasma by week 4 and sustained viremia following AAV8-luciferase treatment for the remaining 22 weeks of the study (Figure 1D). For AAV8-VRC07-treated mice, the bNAb concentration plateaued at a geometric mean of ~55 μg/mL in plasma, which was sustained for the remainder of the study, a value approximately 2,000 times over its *in vitro* IC_{50} value (Figure S1A). Following AAV8-VRC07 treatment, viral loads decreased over a 3-week period, which diverged into two outcomes: viral rebound in 56% (30/54) or sustained control in 44% (24/54) of mice throughout the study (Figures 1E and S1B). Notably, this trend was observed across five independent experiments, each using a unique donor for each batch of BLT mice (Tables S2 and S3).

To explore whether another CD4bs-directed bNAb could achieve long-lived viral suppression, we tested N6,[62] an exceptionally broad bNAb that had an *in vitro* IC_{50} against $HIV_{REJO.c}$ similar to that of VRC07 (Figure 1B; Table S1). In AAV8-N6-treated mice, the plasma concentrations of N6 achieved a geometric mean of ~15 μg/mL, over 300 times above the *in vitro* IC_{50} against $HIV_{REJO.c}$ (Figures 1C and S1A). However, AAV8-N6 treatment only resulted in a transient decline in viral load over the first 2 weeks, which returned to a pre-treatment concentration within 4 weeks of vector injection (Figure 1F).

Finally, we tested PGDM1400,[63] a somatic variant of the PGT145 antibody family that recognizes the HIV envelope trimer V1/V2 apex with exceptional potency. This bNAb neutralized $HIV_{REJO.c}$ with approximately 5-fold greater potency than those measured for VRC07 and N6 (Figure 1B; Table S1). Following AAV8-PGDM1400 administration, serum concentration of PGDM1400 rapidly increased, reaching a geometric mean plasma concentration of ~28 μg/mL, or nearly 3,700 times above the *in vitro* IC_{50} against $HIV_{REJO.c}$ (Figures 1C and S1A). However, all mice treated with AAV8-PGDM1400 displayed no significant change in viremia over the 26-week period of observation (Figure 1G). Only mice receiving AAV8-VRC07 exhibited a significant delay in time to rebound (Figure 1H), and a comparison of the geometric mean viral loads of all evaluated mice demonstrated a significant decline in viral load only for AAV8-VRC07-treated mice compared with AAV8-luciferase control (Figure S1C).

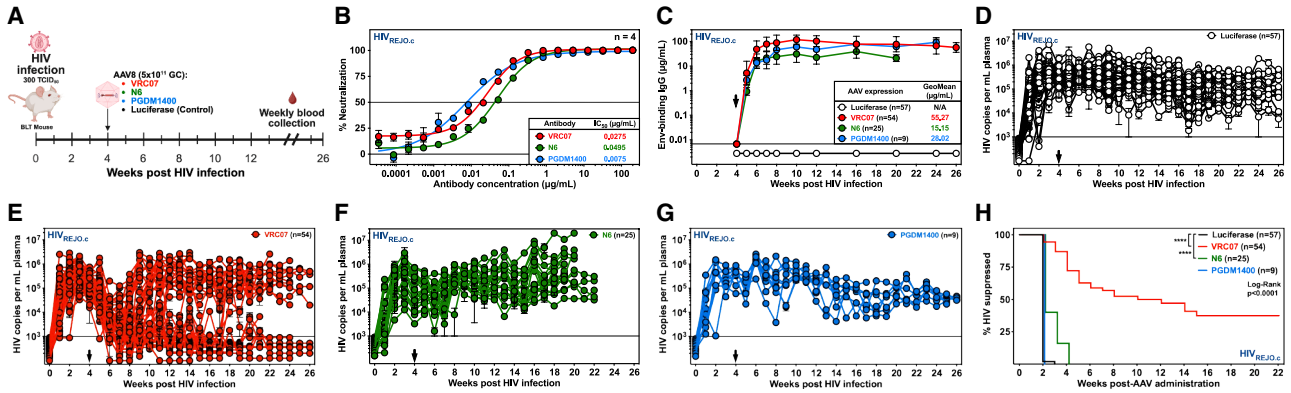

Figure 1. Vectored delivery of VRC07, but not PGDM1400 or N6, can suppress established $HIV_{REJO.c}$ infection

(A) BLT humanized mice were infected with 300 $TCID_{50}$ of $HIV_{REJO.c}$, and the viral population was allowed to replicate for 4 weeks. Mice were then IM injected with 5×10^{11} genome copies (GC) of AAVs encoding for either VRC07, N6, PGDM1400, or luciferase as a control. Mice were followed for 6 months, and blood samples were collected weekly.

(B) *In vitro* neutralization of $HIV_{REJO.c}$ by VRC07, N6, or PGDM1400 bNAbs. Data are plotted as mean ± SEM. Each data point was evaluated in quadruplicate across two independent experiments.

(C) ELISA-based quantitation of gp120-binding antibodies in the serum of $HIV_{REJO.c}$-infected humanized mice following administration of AAV8-luciferase ($n = 57$), AAV8-VRC07 ($n = 54$), AAV8-N6 ($n = 25$), or AAV8-PGDM1400 ($n = 9$) vectors, determined across six independent experiments. A black arrow denotes vector administration. Data are plotted as geometric mean ± geometric SD.

(D–G) HIV viral load in plasma of $HIV_{REJO.c}$-infected mice injected with AAV8-luciferase as a control (D), AAV8-VRC07 (E), AAV8-N6 (F), or AAV8-PGDM1400 (G). Black arrows denote vector administration. Each colored line depicts an individual mouse tracked over time. The sensitivity of qPCR was 1 GC per μL of plasma, and 5 μL were used in the reaction, resulting in a 1,000 copy per mL limit of detection (solid line). Data are presented as mean ± SEM. See also Figure S1.

(H) Kaplan-Meier plot of viral suppression in BLT humanized mice infected with $HIV_{REJO.c}$ given the indicated bNAb-expressing vector. The total model significance ($p < 0.0001$) and pairwise comparison against the luciferase control (****$p < 0.0001$) were assessed independently using log-rank (Mantel-Cox) tests. The percentage of HIV suppressed was defined as the fraction of mice that did not escape as described in the methods.

To control for differences in viral population structure, we compared the average diversity of the HIV *env* gene prior to vector administration and noted no significant differences between the groups (Figure S1D). When comparing AAV8-VRC07-treated mice that did or did not rebound, we found no differences in antibody serum concentration (Figure S1E), but rebounding mice had a 1.6-fold higher viral load compared with suppressed mice (Figure S1F).

The AMP trials identify predicted serum neutralization 80% inhibitory dilution titer (PT_{80}) as a robust predictor of protection in humans and NHPs.[24] A steady-state PT_{80} of 200 or higher correlates with a prevention efficacy of 90%.[24] No differences in PT_{80} among $HIV_{REJO.c}$ suppressed or escaped mice were detected (Figures S1G–S1I). Despite reaching average PT_{80} values against $HIV_{REJO.c}$ of over 500 for VRC07 and over 400 for PGDM1400 over the 4-week period of increasing expression, we did not see efficacy against established infections (Figure S1J).

Together, these data demonstrate that AAV8-mediated delivery of VRC07, but not N6 and PGDM1400, can suppress $HIV_{REJO.c}$ replication in BLT humanized mice.

HIV escape paths are conserved for each bNAb

To understand the basis for the observed variation in bNAb effectiveness against $HIV_{REJO.c}$, we mapped the escape paths traversed by the virus to acquire resistance to each individual bNAb. Env was deep sequencing from plasma viral RNA to analyze non-synonymous mutations that arose during viral escape. Individual control mice exhibited mutations distributed throughout the $HIV_{REJO.c}$ envelope (Figure S2A, control); however, these mutations followed no discernible pattern (Figure S2B) and did not impact potential N-linked glycosylation sites (PNGs) (Figure S2C).

Most Env sequences obtained from $HIV_{REJO.c}$-infected animals that escaped from VRC07 exhibited two pairs of potential escape mutations: either two D-loop mutations (N276D and D279A) or a D-loop and a V5-loop mutation (D279A and N460D, respectively) (Figure S2A, VRC07). When assessed collectively across all escaped mice, these three mutations encompassed the majority of amino acid divergence from the parental (wild-type [WT]) sequence (Figure 2A). Notably, the N460D mutation also resulted in a PNG loss in the V5-loop of $HIV_{REJO.c}$ (Figure S2D).

To determine the impact of these mutations on VRC07 resistance, each Env mutation was engineered into an $HIV_{REJO.c}$ IMC plasmid to produce replication-competent viruses, which were tested for neutralization sensitivity against VRC07 *in vitro* (Figure 2B). When assessed individually, neither N276D nor N460D conferred any resistance to VRC07 neutralization relative to the WT $HIV_{REJO.c}$. However, D279A led to partial escape by mediating a 51-fold increase in the IC_{50} to 1.4 μg/mL and a reduction of the dose-response curve slope (Table S1).[64] Of note, the D279A $HIV_{REJO.c}$ IC_{50} remained well below the geometric mean serum concentration of VRC07 achieved *in vivo*. However, complete escape from VRC07 was only observed for envelopes containing both D279A and either N460D or N276D (Figure 2B).

To measure the fitness cost associated with VRC07 escape mutations emerging in $HIV_{REJO.c}$, we determined the growth rate of each IMC envelope mutant using *QuickFit* (Figure S2E).[65]

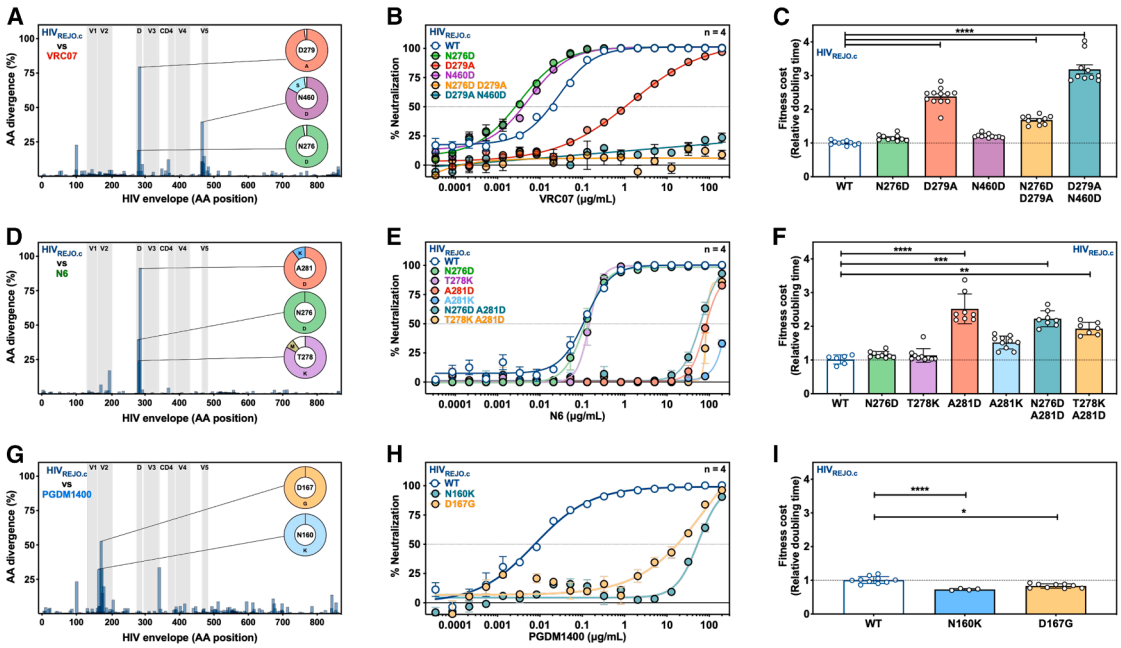

Figure 2. $HIV_{REJO.c}$ escapes from each bNAb by finding conserved mutations with specific fitness costs and resistance benefits

(A, D, and G) Amino acid divergence from the envelope gene of the $HIV_{REJO.c}$ parental strain across AAV8-VRC07 (A) (n = 27), AAV8-N6 (D) (n = 22), and AAV8-PGDM1400 (G) (n = 9) treated mice, determined throughout six independent experiments. Sequences were determined by Illumina Deep Sequencing of the viral envelope isolated from plasma at the final experimental time point. The x axis represents the envelope protein amino acid position relative to HIV_{HXB2} numbering. The y axis represents the percentage of average amino acid divergence from the parental strain, corrected for divergence observed in control mice. Pie charts represent the most common amino acid mutations for sites with the highest divergence. See also Figure S2.

(B, E, and H) *In vitro* neutralization assays of each $HIV_{REJO.c}$ mutant identified in (A), (D), and (G) against each corresponding bNAb. Data are plotted as mean ± SEM. Each data point was evaluated in quadruplicate across three independent experiments.

(C, F, and I) Relative viral growth of each $HIV_{REJO.c}$ mutant identified in (A), (D), and (G). Growth rates were determined in activated $CD4^+$ T cells performing *QuickFit* assays and normalized to the parental strain. Each mutant was measured in two independent experiments with at least two replicates per experiment. Data are plotted as mean ± SEM, and statistical differences were assessed by a Kruskal-Wallis non-parametric ANOVA with Dunn's post hoc test to correct for multiple comparisons (****$p < 0.0001$).

See also Figure S2.

The D279A mutation incurred a significant fitness cost, whereas no changes were observed for the N276D or N460D mutations alone (Figure 2C). Strains containing paired mutations exhibited a higher fitness cost compared with the WT strain.

The escape paths traversed by $HIV_{REJO.c}$ to acquire resistance to N6 were also evaluated (Figure S2A, N6). Three mutations in or around the D-loop were the most frequent (Figure 2D), with one of them resulting in the loss of a PNG (Figure S2F). Unlike VRC07, one mutation in the D-loop, A281D, was sufficient to escape N6 (Figure 2E; Table S1). Additionally, A281K led to complete escape from N6, although it required three nucleotide mutations from the parental sequence (Figure 2E). Using QuickFit, we found that the initial A281D and the combinations with N276D or T278K resulted in a higher fitness cost relative to the WT strain (Figures 2F and S2G).

The PGDM1400 escape mutations were observed surrounding the V1/V2 trimer apex region, with N160K and D167G being the most prevalent (Figures 2G and S2A, PGDM1400), and with the former resulting in the loss of PNGs (Figure S2H). As expected, both of these mutations were sufficient to confer complete resistance to PGDM1400 (Figure 2H; Table S1). Acquisition of mutations N160K and D167G resulted in a fitness benefit compared with the WT strain (Figures 2I and S2I).

Together, these data demonstrate that $HIV_{REJO.c}$ escape mutations are specific to each bNAb and are generally limited to a conserved set of escape paths.

The escape barrier of each bNAb is determined by the fitness landscape of escape paths

To understand why a given pathway was traversed as opposed to another, we created an escapability map of the fitness landscape in the context of VIT (Figure S2P). We projected individual escape mutations onto a two-dimensional axis of replicative fitness cost and resistance benefit. This was done for each bNAb, with each point representing an identified escape mutation and arrows representing the potential escape paths (Figures 2A–2C). We categorized each mouse sample into an escape path by using the viral haplotype frequencies of the dominant escape mutations (Figures S2K–S2P).

Notably, 81% of the $HIV_{REJO.c}$ sequences harbored the D279A mutation, conferring partial escape from VRC07, albeit with a high fitness cost (Figure 2A). These escaped viruses also acquired a secondary mutation, typically N460D (path A) or N276D (path B), leading to complete escape from VRC07. Path A escape variants (D279A + N460D) incurred an even higher fitness cost than the D279A-only escape variants, whereas

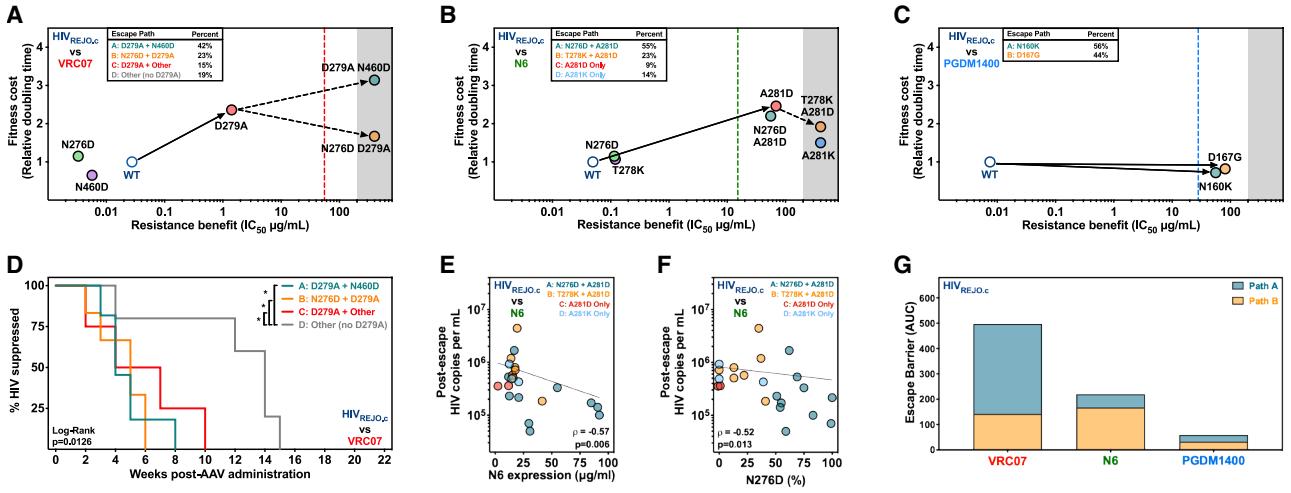

Figure 3. The difficulty of escape from each bNAb is determined by the escapability of each HIV_{REJO} mutation accrued along the escape paths

(A–C) Escapability maps denoting fitness cost (*y* axis, relative doubling time shown in Figure 2) and resistance benefits (*x* axis, neutralization resistance shown in Figure 2) for each $HIV_{REJO.c}$ mutant observed during escape from VRC07 (A), N6 (B), or PGDM1400 (C). Dashed vertical lines denote the geometric mean antibody serum concentration after vectored bNAb administration. Shaded areas represent the neutralization assay limit of detection. Solid arrows represent the likely initial path taken, and dashed arrows represent the likely second step to escape. In the map legend, each escape path is sorted based on the relative frequency observed in the sequencing data. See also Figure S2.

(D) Survival analysis of $HIV_{REJO.c}$-infected mice treated with AAV8-VRC07 by escape path haplotype. The total model significance ($p = 0.0126$) and pairwise comparisons of the non-D279A escape paths to each other escape path ($^*p < 0.05$) were assessed independently using log-rank (Mantel-Cox) tests. A total of 25 mice were evaluated across six independent experiments. See also Figure S2.

(E) Correlation plot of N6 geometric mean expression vs. post-escape $HIV_{REJO.c}$ viral load. The line represents the semi-log least squares regression, and ρ represents the Spearman correlation value determined for the data, with the associated *p* value below. A total of 22 mice were evaluated across six independent experiments. See also Figure S2.

(F) Correlation plot of the post-N6 escape viral load of $HIV_{REJO.c}$ vs. the frequency of N276D determined by viral envelope sequencing. The line represents the semi-log least squares regression, and ρ represents the Spearman correlation value determined for the data, with the associated *p* value below. A total of 22 mice were evaluated across six independent experiments. See also Figure S2.

(G) Escape barrier (AUC) score denoting the aggregate fitness cost for each escape path as determined in the escapability maps. This score was calculated by adding the area under the escapability plot for escape paths A and B viral escapes from VRC07, N6, and PGDM1400.

See also Figure S2.

path B escape variants (N276D + D279A) improved their fitness relative to the D279A-only variants. The remaining 19% of the escapes did not harbor the D279A amino acid change as a partial escape (path D), but rather found an alternative escape pathway. These non-canonical escape paths exhibited a significant delay in time to escape (Figure 2D), suggesting that these viral populations incurred a higher fitness cost than D279A-based escape paths. To identify the forces driving a given population into a specific path, we compared the VRC07 serum concentration (Figure S2Q), the post-escape viral load (Figure S2T), and the total number of accumulated mutations (Figure S2W) for each path but failed to find any significant differences across the paths.

The same analysis was performed for N6 (Figure 3B), where 86% of the escape variants harbored an A281D mutation, conferring complete escape from N6. These A281D variants typically had a second mutation, either N276D (path A) or T278K (path B). Compared with A281D-only variants, path A escapes were marginally more fit and less resistant to N6, while path B escapes were more fit and more resistant to N6 (Figure 3B). A mix of both path A and path B haplotypes was found within most samples (Figure S2O). Notably, samples with higher serum concentrations of N6 were associated with lower post-escape viral loads (Figure 3E), suggesting that N6 may impair viral replication. This was particularly evident for samples with higher frequencies of N276D (path A) (Figure 3F). There were also some samples harboring only the A281D variant, with no other prevalent mutations; however, the N6 serum concentration of these samples was 6.4-fold lower compared with those of path A samples (Figure S2R). Of note, given that there were only two samples, statistical differences could not be assessed. The post-escape viral load (Figure S2U) and the total number of accumulated mutations (Figure S2X) were similar across the different paths.

Finally, the PGDM1400 escape paths were clustered based on the haplotypes of N160K and D167G (Figures 3C, S2M, and S2P). N160K (path A) was found in 56% of the escape variants, and the remaining 44% contained D167G (path B). Both paths led to complete escape from PGDM1400 (Figure 3C). We did not observe significant differences between the PGDM1400 serum concentrations and post-escape viral loads for the two escape paths (Figures S2S and 2V, respectively). However, path B escapes accumulated significantly more mutations compared with path A escapes (Figure S2Y).

To understand the cumulative fitness cost of $HIV_{REJO.c}$ escape from VRC07, N6, and PGDM1400, we determined escape barrier scores by calculating the area under the curve (AUC) of the escapability maps (Figures S2Z–S2AB). We then combined the

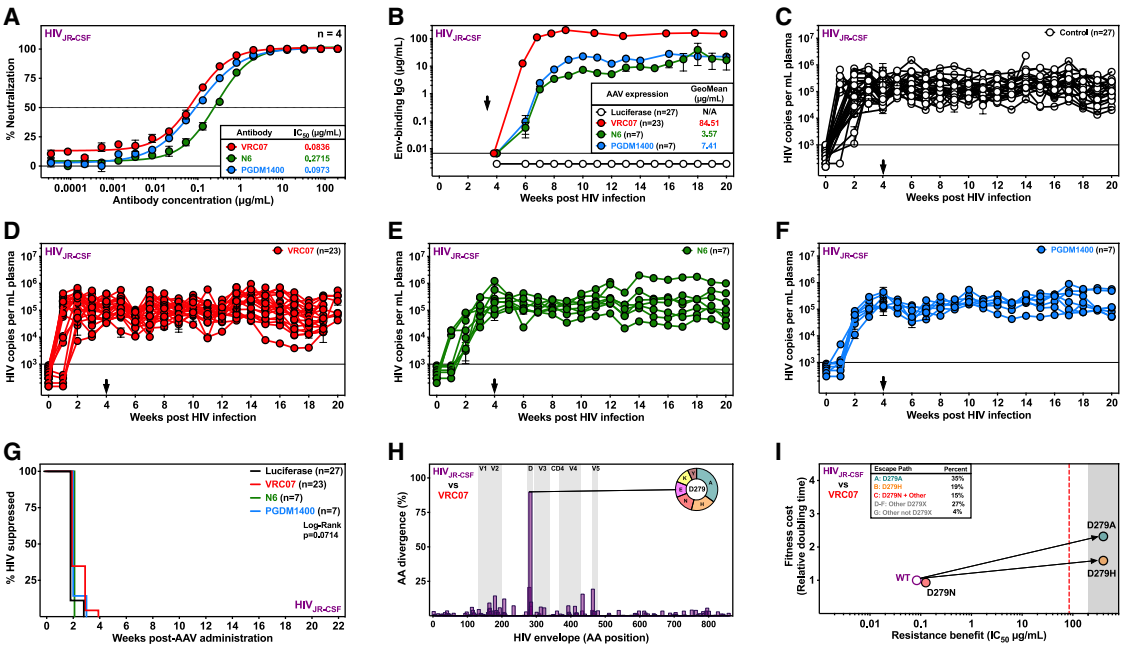

Figure 4. HIV_{JR-CSF} escapes vectored delivery of individual bNAbs by acquiring mutations similar to those seen for $HIV_{REJO.c}$

(A) *In vitro* neutralization of HIV_{JR-CSF} by VRC07, N6, or PGDM1400 bNAbs. Data are plotted as mean ± SEM. Each data point was evaluated in quadruplicate across two independent experiments.

(B) ELISA-based quantitation of gp120-binding antibodies in the serum of HIV_{JR-CSF}-infected humanized mice following administration of 5×10^{11} genome copies (GCs) of AAV8-luciferase ($n = 27$), AAV8-VRC07 ($n = 23$), AAV8-N6 ($n = 7$), or AAV8-PGDM1400 ($n = 7$) vectors, determined across three independent experiments. A black arrow denotes vector administration. Data are plotted as geometric mean ± geometric SD.

(C-F) HIV viral load in plasma of HIV_{JR-CSF}-infected mice injected with AAV8-luciferase as control (C), AAV8-VRC07 (D), AAV8-N6 (E), or AAV8-PGDM1400 (F). Black arrows denote vector administration. Each colored line depicts an individual mouse tracked over time. The sensitivity of qPCR was 1 GC per μL of plasma, and 5 μL were used in the reaction, resulting in a 1,000 copy per mL limit of detection (solid line). Data are presented as mean ± SEM. See also Figure S3.

(G) Kaplan-Meier plot of viral suppression in humanized mice infected with HIV_{JR-CSF} given the indicated bNAb-expressing vector. The total model significance was assessed using a log-rank (Mantel-Cox) test ($p = 0.0714$).

(H) Amino acid divergence from the envelope gene of the HIV_{JR-CSF} parental strain across AAV8-VRC07-treated mice ($n = 20$) throughout three independent experiments. Sequences were determined by Illumina Deep Sequencing of the viral envelope isolated from plasma at the final experimental time point. The *x* axis represents the envelope protein amino acid position relative to HIV_{HXB2} numbering. The *y* axis represents the percentage of average amino acid divergence from the parental strain, corrected for divergence observed in control mice. The pie chart represents the most common amino acid mutations for the site with the highest divergence. See also Figure S3.

(I) Escapability map of HIV_{JR-CSF} escape from VRC07. The dashed vertical line denotes the geometric mean antibody serum concentration after AAV8-VRC07 administration. The shaded area represents the neutralization assay limit of detection. Arrows represent the likely path taken to escape.

See also Figure S3.

AUC of the top two escape paths, accounting for the majority of the observed haplotypes, into a final escape barrier score (Figures S2AC–S2AE). Interestingly, the ranking of the escape barrier scores for VRC07, N6, and PGDM1400 corresponded with *in vivo* experimental outcomes (Figure 3G).

Together, these data profile the fitness cost and resistance benefit of each major escape path and demonstrate how these values determine the escape barrier score.

HIV_{JR-CSF} rapidly escapes from bNAbs due to low-fitness-cost escape mutations

Given the ability of AAV8-VRC07 to reproducibly suppress $HIV_{REJO.c}$ in a subset of mice, we determined whether this could be replicated with HIV_{JR-CSF}, a tier 2, clade B, CCR5-tropic primary isolate originally obtained from the cerebrospinal fluid of a person living with HIV.[55] Humanized mice were infected with an HIV_{JR-CSF} prior to receiving AAV8-luciferase or AAV8-bNAbs (Tables S2 and S3). Antibody expression stabilized within 4 weeks of AAV administration, achieving geometric mean plasma concentrations tens to hundreds of times above the *in vitro* IC_{50} (Figures 4A, 4B, and S3A). In contrast to $HIV_{REJO.c}$, HIV_{JR-CSF}-infected mice exhibited no changes in viral load following administration of any of the AAV8-bNAbs evaluated and were indistinguishable from the AAV8-luciferase controls (Figures 4C–4G).

We deep sequenced HIV_{JR-CSF} Env from each mouse to identify mutations associated with escape from VRC07, N6, and PGDM1400 (Figure S3B). Mice receiving AAV8-luciferase exhibited consistent mutations in Env, despite the absence of bNAb selection pressure, suggesting adaptation to the host (Figure S3C), such as N339, which translated into the loss of PNGs near the V3-loop and was not observed for $HIV_{REJO.c}$ (Figure S3D).

HIV_{JR-CSF} escaped from VRC07 by acquiring a single D-loop mutation at position D279 (Figure 4H), and a minority of samples exhibited a loss of PNGs at N276 (Figure S3E). The D279A and

D279H mutations achieved complete escape from VRC07 (Figure S3F; Table S1). D279A increased fitness cost, while D279H and D279N had no change in fitness (Figures S3G and S3H). A single mutation at site D279 was sufficient to mediate complete escape from VRC07 with a modest fitness cost (Figure 4I).

Next, we evaluated the escape paths for N6 and found a single nucleotide change to A281D (Figure S3I), along with the loss of PNGs at site N276 (Figure S3J). The A281D mutation was sufficient to achieve escape (Figure S3K), albeit at a high fitness cost (Figures S3L and S3M). We observed that the combination of A281D with N276D resulted in complete escape at a lower fitness cost (Figure S3N).

Finally, escape from AAV8-PGDM1400 treatment resulted in a variety of V2-loop mutations at sites N160 or T162 (Figure S3O), resulting in loss of a PNGs (Figure S3P). All of these mutations resulted in escape from PGDM1400 (Figure S3Q), with no fitness cost (Figures S3R–S3T).

To confirm the activity of the expressed bNAbs *in vivo*, we evaluated the neutralizing activity of sera from a subset of these animals (Figures S4A–S4H). The tested sera neutralized $HIV_{REJO.c}$ and $HIV_{JR\text{-}CSF}$ with IC_{50} values similar to purified proteins. No neutralization activity was seen in sera from control mice.

To explore whether the kinetics of vectored antibody expression played a role in the lack of antiviral activity seen for N6 and PGDM1400 in our studies, we performed passive transfer of either a control antibody (2A10), N6, or PGDM1400 in $HIV_{JR\text{-}CSF}$-infected humanized mice (Figures S4I–S4L; Tables S2 and S3). High antibody concentrations were detected as early as 1 week post-infusions (Figure S4I); however, we did not observe changes in viral load (Figures S4K and S4L) and no delay in viral escape (Figure S4M). Deep sequencing revealed the selection of escape mutations that mirrored those seen for AAV-delivered bNAbs (Figures 4N–4P), suggesting that differences in antibody expression kinetics do not explain the lack of activity seen in our studies.

These data demonstrate how low-fitness-cost escape paths allow $HIV_{JR\text{-}CSF}$ to readily escape from AAV-mediated VRC07, N6, and PGDM1400.

Increasing $HIV_{REJO.c}$ mutation resistance benefit enables complete escape from VRC07

To evaluate whether the inherent fitness of the Env sequence of each isolate impacted escapability, we compared the baseline frequency of each amino acid in *env* for both isolates to the frequencies observed in clinical isolates found in the LANL database. Amino acid frequencies in $HIV_{REJO.c}$- and $HIV_{JR\text{-}CSF}$-infected BLT mice mirrored those found in the LANL database (Figure S4Q; Table S4). We then compared the LANL amino acid frequency of each escape mutation observed in humanized mice to their fitness cost by QuickFit and found a significant negative correlation (Figure S4R), confirming that rare mutations in the LANL database have a high fitness cost in humanized mice.

To understand the contribution of the resistance benefit independent of fitness cost, we engineered chimeric IMCs of $HIV_{REJO.c}$ containing swaps of sequences comprising the D-loop (HIV_{RD}), the V5-loop (HIV_{RV}), or both (HIV_{RDV}) from $HIV_{JR\text{-}CSF}$ (Figure 5A; Tables S2 and S3). All three chimeras were neutralized by VRC07 similarly to the original isolates (Figure 5B). Importantly, HIV_{RV} showed no difference in fitness relative to the $HIV_{REJO.c}$ strain (Figures S5A and S5B).

Following infection of BLT humanized mice with chimeric strains, AAV8-VRC07 administration resulted in a plasma antibody concentration of approximately 50 μg/mL (Figure 5C). This led to suppression in a subset of $HIV_{REJO.c}$-infected mice, whereas all $HIV_{JR\text{-}CSF}$-infected mice escaped (Figures S5C and S5D). A similar proportion of mice infected with HIV_{RD} and HIV_{RDV} were suppressed by VRC07, as seen for $HIV_{REJO.c}$ (Figures S5E and S5F). By contrast, all mice infected with HIV_{RV} exhibited rapid escape from VRC07, as seen for $HIV_{JR\text{-}CSF}$ (Figures 5D, S5G, and S5H).

We focused on the HIV_{RV} chimera to understand why this swap resulted in a suppression outcome similar to that of $HIV_{JR\text{-}CSF}$. In contrast to $HIV_{REJO.c}$, mutations arising in HIV_{RV}-infected animals receiving AAV8-VRC07 were confined to the D-loop (Figures 5E and S5I–S5L). HIV_{RV} mutants harboring single amino acid changes at D279 completely escaped from VRC07, albeit with substantial fitness costs (Figures 5F, 5G, and S9M).

The escapability map revealed that D279 mutations resulted in complete escape for HIV_{RV}, in contrast to $HIV_{REJO.c}$ (Figure 5H). Finally, the escape barrier score for $HIV_{JR\text{-}CSF}$ escaping from all bNAbs and HIV_{RV} escape from VRC07 was calculated as before (Figures S5N–S5Q). For $HIV_{JR\text{-}CSF}$, VRC07 exhibited the lowest score, whereas the HIV_{RV} score was between $HIV_{REJO.c}$ and $HIV_{JR\text{-}CSF}$ (Figures 5I, S5R, and S5S).

Taken together, these data suggest that the sequence context of the HIV envelope directly influences the path taken to escape from VRC07.

Increasing $HIV_{REJO.c}$ mutation fitness cost results in complete suppression by VRC07

To evaluate the impact of mutation fitness cost on escape, we altered the fitness of VRC07-escape mutants without changing their resistance benefits. Given the known reduction in viral fitness due to polymerase (Pol) mutations selected during escape from ART,[66] we tested the effect of combining VRC07 escape mutations with mutations in Pol. Interestingly, when tested in the WT background, Pol M184I and M184V led to no changes in neutralization sensitivity to VRC07 or viral fitness (Figures S6A and S6B). We then evaluated the VRC07-$HIV_{REJO.c}$ escape mutations in the context of the Pol M184V mutation. While there were no changes in neutralization sensitivity (Figures 2B and S6C; Table S1), we observed significant increases in the fitness cost for escape mutants containing Pol M184V relative to WT (Figures 4A and S6D). This resulted in a shift in the escapability map for $HIV_{REJO.c}$ with the Pol M184V mutation, where complete escape through a second envelope mutation incurred substantially higher fitness costs than for the WT Pol strain (Figure 6B). The escape barrier score for Pol M184V mutants was higher when assuming the same escape path frequencies seen for the WT Pol (Figure 6C), suggesting that selection of the Pol M184 mutations might improve VRC07 suppression of $HIV_{REJO.c}$.

To test this, we intentionally drove the emergence of Pol mutations through suboptimal dosing of ART in humanized mice. Mice were infected with $HIV_{REJO.c}$, and we slowly increased

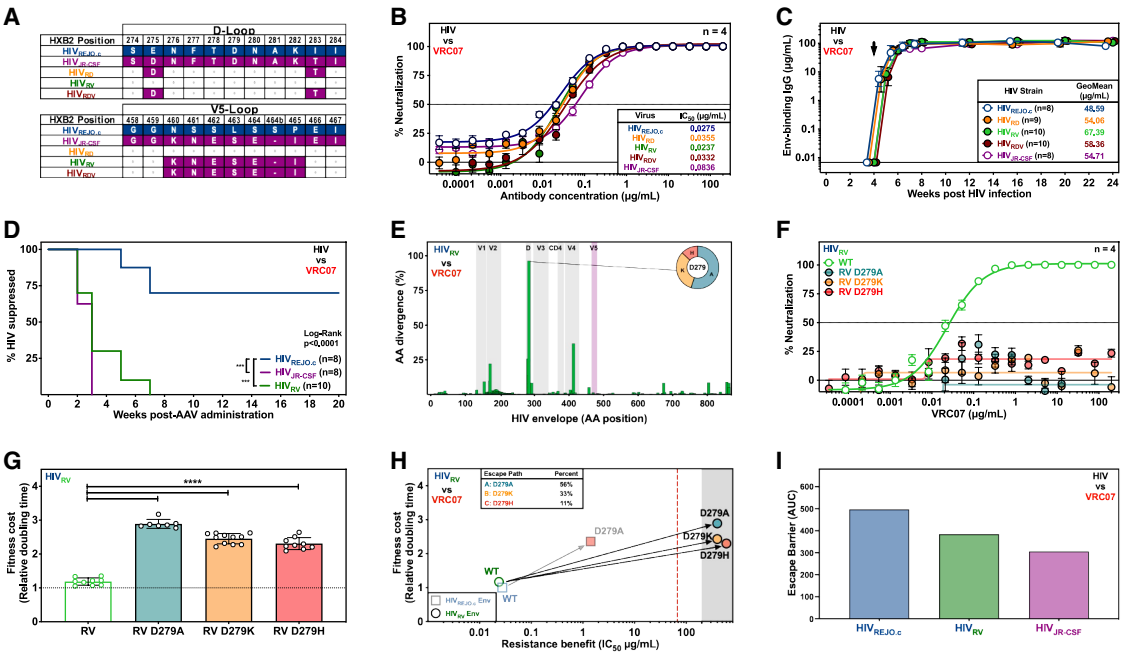

Figure 5. $HIV_{REJO.c}$ V5-loop restricts escape from VRC07 by decreasing the resistance benefit of D279 mutations

(A) Alignment of the D-loop and the V5-loop amino acid sequences for $HIV_{REJO.c}$, HIV_{JR-CSF}, and the HIV_{RD}, HIV_{RV}, and HIV_{RDV} chimeras. See also Figure S5.

(B) *In vitro* neutralization of $HIV_{REJO.c}$, HIV_{RD}, HIV_{RV}, HIV_{RDV}, and HIV_{JR-CSF} by VRC07 bNAb. Data are plotted as mean ± SEM. Each data point was evaluated in quadruplicate across two independent experiments.

(C) ELISA-based quantitation of gp120-binding antibodies in the serum of $HIV_{REJO.c}$ (n = 8), HIV_{JR-CSF} (n = 8), HIV_{RD} (n = 9), HIV_{RV} (n = 10), and HIV_{RDV} (n = 10) infected humanized mice following administration of 5×10^{11} genome copies (GCs) of AAV-luciferase or AAV-VRC07 in a single independent experiment. A black arrow denotes vector administration. Data are plotted as geometric mean ± geometric SD.

(D) Kaplan-Meier plot of viral suppression in humanized mice infected with $HIV_{REJO.c}$, HIV_{RV}, or HIV_{JR-CSF} following vectored VRC07 administration. The total model significance ($p < 0.0001$) and pairwise comparisons against $HIV_{REJO.c}$ (***$p < 0.001$) were assessed independently using log-rank (Mantel-Cox) tests. See also Figure S5.

(E) Amino acid divergence from the envelope gene of the HIV_{RV} parental strain across AAV8-VRC07-treated mice (n = 9) in a single independent experiment. Sequences were determined by Illumina Deep Sequencing of the viral envelope isolated from plasma at the final experimental time point. The x axis represents the envelope protein amino acid position relative to HIV_{HXB2} numbering. The y axis represents the percentage of average amino acid divergence from the parental strain, corrected for divergence observed in control mice. The pie chart represents the most common amino acid mutations for the site with the highest divergence. See also Figure S5.

(F) *In vitro* neutralization assay of HIV_{RV} mutants identified as potential VRC07 escapes against VRC07. Data are plotted as mean ± SEM. Each data point was evaluated in quadruplicate across two independent experiments.

(G) Relative viral growth of HIV_{RV} mutants identified as potential VRC07 escapes using the *QuickFit* assay. Each mutant was measured in two independent experiments with at least two replicates per experiment. Data are plotted as mean ± SEM, and statistical differences were assessed by a Kruskal-Wallis non-parametric ANOVA with Dunn's post hoc test to correct for multiple comparisons (****$p < 0.0001$). See also Figure S5.

(H) Escapability map of HIV_{RV} during escape from VRC07. Lighter square symbols represent the original $HIV_{REJO.c}$ escape path taken against VRC07. The dashed vertical line denotes geometric mean bNAb concentrations after vectored VRC07 administration. Shaded areas represent the limits of detection. Arrows represent the likely path to escape. See also Figure S5.

(I) Escape barrier (AUC) score quantifying the difficulty of escape from VRC07 for $HIV_{REJO.c}$, HIV_{RV}, and HIV_{JR-CSF}. See also Figure S5.

the dose of ART drug in their food, from 1% to 100% of the standard human equivalent dose over 6 weeks. 8 weeks after infection, AAV8-VRC07 or AAV8-luciferase was administered. 2 weeks after AAV administration, the ART treatment was interrupted (Figure 6D; Tables S2 and S3). Importantly, at the time of AAV administration, no meaningful differences in viral loads were seen between the mice that had received escalating ART relative to control mice (Figure S6E). As expected, HIV *pol* genes sequenced from mice receiving the suboptimal ART dosing displayed a near-complete prevalence of M184V/I at the time of VRC07 administration (Figure 6E).

As anticipated, ART drug treatment had no impact on AAV8-driven expression of VRC07 (Figure S6F). Administration of AAV8-VRC07 without ART treatment resulted in only partial suppression of HIV, as observed in our prior experiments (Figure S6G). Additionally, the post-escape viral load for the luciferase-treated mice showed no difference irrespective of the presence or absence of the selective pressure (Figure S6H). ART-treated mice receiving AAV8-luciferase maintained steady viral loads (Figure S6I). Administration of AAV8-VRC07 to ART-treated mice resulted in complete suppression of $HIV_{REJO.c}$ (Figures 6F and 6G).

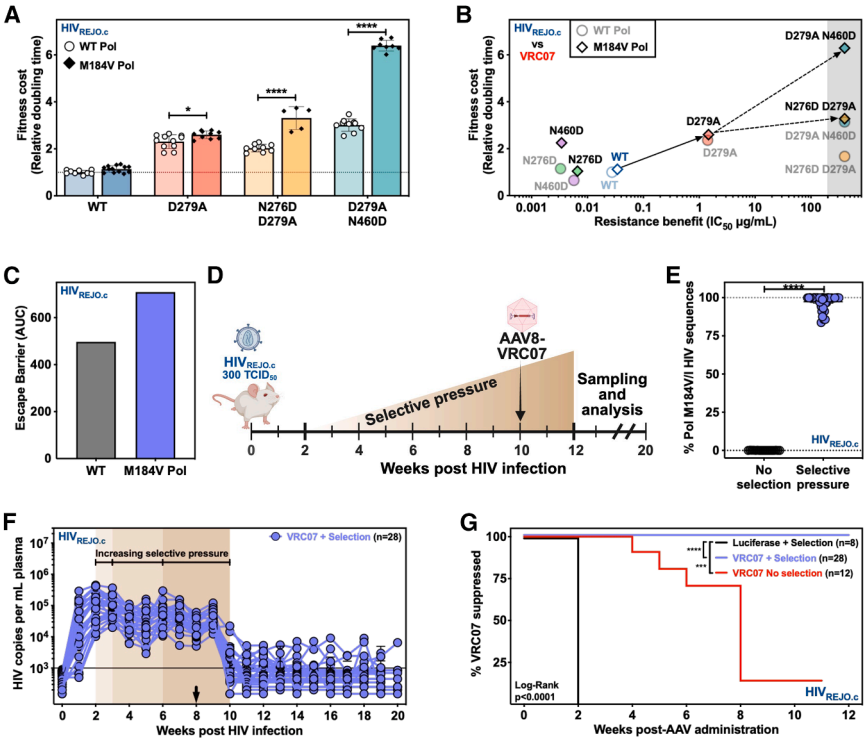

Figure 6. Increasing the fitness cost of $HIV_{REJO.c}$ escape mutations enhances the efficacy of vectored VRC07

(A) The fitness of $HIV_{REJO.c}$-VRC07 escape mutations with or without the Pol M184V mutation was evaluated using *QuickFit*. Each mutant was measured in two independent experiments with at least two replicates per experiment. Data are presented as mean ± SD. Statistical differences were assessed by a two-way ANOVA, with a Šidák post hoc test to correct for multiple comparisons (*$p < 0.05$; ****$p < 0.0001$). See also Figure S6.

(B) Escapability map of $HIV_{REJO.c}$-VRC07 escape mutants with or without the Pol M184V mutation. Solid symbols (diamonds) represent envelope mutations on the Pol M184V mutant background, while lighter symbols (circles) represent the data for envelope mutations on the WT Pol background. Shaded areas represent the limits of detection. Solid arrows represent the likely path taken, with dashed arrows representing secondary steps to escape. See also Figure S6.

(C) Empirical escape barrier score for $HIV_{REJO.c}$ escape from VRC07 as compared with the theoretical escape barrier score for $HIV_{REJO.c\text{-}PolM184V}$ escape from VRC07.

(D) Experimental setup to determine the impact of Pol M184 mutations on $HIV_{REJO.c}$ escape from VRC07. Humanized mice were infected with $HIV_{REJO.c}$ and then treated with a suboptimal ART starting 2 weeks after infection to select and maintain Pol M184 mutants. At week 8, 5×10^{11} GC of AAV8-VRC07 was injected IM, and the ART regimen was stopped at week 10. Mice were followed for 6 months, and blood samples were collected weekly.

(E) Percentage of Pol M184V/I mutations determined from viral sequences isolated from the plasma of $HIV_{REJO.c}$-infected mice at week 8, prior to AAV8-VRC07 administration, with ($n = 36$) or without ($n = 20$) selective pressure induced by ART. Statistical differences were assessed by an unpaired two-tailed Student's *t* test (****$p < 0.0001$). Data are presented as mean ± SEM.

(F) $HIV_{REJO.c}$ viral load in plasma of AAV8-VRC07-treated mice ($n = 28$) in a single independent experiment. Black arrows denote vector administration. Each colored line depicts an individual mouse. The qPCR lower limit of detection was 1 GC per µL of plasma, and 5 µL were used in the reaction (solid line). Data are presented as mean ± SEM.

(G) Kaplan-Meier plot of viral suppression in humanized mice infected with $HIV_{REJO.c}$ with or without ART selection and with or without AAV8-VRC07 administration. The total model significance ($p < 0.0001$) and pairwise comparisons against the luciferase + selection control (***$p < 0.001$; ****$p < 0.0001$) were assessed independently with log-rank (Mantel-Cox) tests.

See also Figure S6.

Taken together, these results suggest that decreasing the overall fitness of $HIV_{REJO.c}$, therefore modulating the fitness cost axis of the escapability maps, makes resistance to VRC07 significantly more difficult.

DISCUSSION

Antibody immunotherapy to prevent or treat HIV infection is being evaluated in numerous clinical trials. While bNAb combinations show promise,[38,42,67,68] individual bNAbs have limited activity in viremic PLWH due to their half-life and the emergence of escape mutations.[34,35,37,39,69,70] Here, we showed that vectored delivery of a single bNAb, well-matched to the infecting strain, is capable of suppressing viremia in approximately half of HIV-infected humanized mice. Notably, this efficacy was not correlated with neutralization potency determined *in vitro* against the infecting viral stock or breadth metrics derived from global pseudovirus panels.[17,62,63] Rather, our results suggested that the *in vivo* efficacy of this treatment is best explained by the bNAb-specific dynamics of viral escape. Using BLT humanized mice and viral stocks derived from IMCs, we performed dozens of independent infections with a specific virus and AAV8-bNAb treatment. This led to reproducible elicitation of the most commonly traversed escape paths by HIV, demonstrating conservation of viral escape from specific bNAbs.

Of the two CD4bs-targeting antibodies evaluated in this study, N6 is broader, neutralizing 96% of a 181-strain global panel with an IC_{50} of less than 1 µg/mL.[62] Despite its outstanding potency and breadth, a single base pair change in the D-loop of $HIV_{REJO.c}$ or $HIV_{JR\text{-}CSF}$ yielded resistance to neutralization. This A281 mutation is also reported for antibodies from the VRC01-class family, which suggests conserved escape paths for these antibodies.[71,72] However, expression was low relative to other bNAbs despite identical vector dosage, consistent with previous reports of short N6 half-life following passive transfer.[73,74] Despite a lack of viral suppression by AAV8-N6, we observed that mice with higher antibody concentrations exhibited lower post-escape viral loads, suggesting that higher steady-state concentrations of N6 may achieve viral suppression.

PGDM1400 recognizes the HIV envelope V1/V2 trimer apex and neutralizes it with a median IC_{50} of 0.003 µg/mL against a 77-virus panel.[63] A single-point mutation in the V2-loop

(N160 or D167) led to complete resistance to PGDM1400, as seen previously for trimer apex-targeting antibodies.[75] The low fitness cost of these mutations was reflected in their high pre-existing frequency in control mice and PLWH. In a clinical trial using PGDM1400, multiple sequences isolated from rebound participants exhibit a loss of the N160 glycan, which suggests that glycan-based escape is a major driver of bNAb resistance in humans.[67]

VRC07 neutralizes 83% of a panel of 179 strains at less than 1 μg/mL, with a geometric mean IC_{50} of 0.11 μg/mL.[17] In contrast to N6 and PGDM1400, complete escape of $HIV_{REJO.c}$ from VRC07 required two steps. The mutations reported here include an essential D-loop mutation at D279, resulting in partial resistance with moderate fitness cost, and a second mutation in either the D- or V5-loops, which confers complete resistance and further modulates the fitness of the virus. Notably, the tolerability of D- and V5-loop mutations identified through deep mutational scanning varies across strains, in line with our isolate-specific fitness cost data.[76] Of note, the N276D D279A escape path was observed less often than the D279A N460D path, despite having a lower fitness cost. This may be a result of the high frequency of pre-existing N460D and the large distance between these two mutations, which increases the likelihood of recombination.[77] Of note, D279A, along with the paired mutations at N276 and N460, are reported escape mutations from VRC01-class antibodies in humans.[36,72,78] Finally, $HIV_{REJO.c}$ escapes that did not acquire D279A exhibited a statistically significant delay in time-to-escape, suggesting that blocking a primary escape path can result in the emergence of more costly alternatives. Of note, there were no differences in PT_{80} values between $HIV_{REJO.c}$ suppressed or escaped mice, demonstrating that in our model, potency- and breadth-derived parameters were insufficient to predict the *in vivo* efficacy of bNAbs.[24,79]

Our results showed that escape from CD4bs-directed bNAbs was more likely to impact viral fitness as compared with bNAbs targeting a variable loop, likely due to the CD4-binding requirement during viral infection.[36,80] In a clinical trial evaluating 3BNC117, another CD4bs-targeting bNAb, sequences from three out of eight participants remain sensitive to the bNAb following viral rebound after antibody serum decay.[34] Recent characterization of escape from eCD4-Ig further demonstrates the difficulty of viral escape from CD4bs-targeted therapeutics.[80] Collectively, our results and these findings highlight the advantage of targeting high fitness-cost epitopes.

In this study, we projected the fitness landscape of each bNAb strain onto two-dimensional escapability maps by comparing both the fitness cost and resistance benefit of mutations. Using chimeric strains, we modulated the neutralization benefit of escape mutations as represented by the *x* axis of the escapability maps. Despite the same neutralization sensitivity to VRC07 and no difference in fitness compared with $HIV_{REJO.c}$, we found that the HIV_{RV} chimera exhibited complete and rapid escape from vectored VRC07, like HIV_{JR-CSF}, highlighting the importance of sequence context on escape.[76] In this study, we utilized two HIV isolates and found that the diversity of the quasispecies in infected humanized mice was similar to the sequence diversity seen in the LANL database, as reported by other studies that evaluated the conservation of mutations cross-sectionally.[81] Importantly, this conservation also correlated with our measured fitness cost of the mutations, showing that more costly mutations were infrequent in the LANL database. The relevance of the sequence context and diversification could have implications for studies performed in NHPs, given the chimeric nature of SHIV.[82]

We also modulated the fitness cost of escape mutations, as represented by the *y* axis of the escapability maps. We found that Pol mutant viruses harboring VRC07 escape mutations maintained their susceptibility to VRC07 but were less fit than WT Pol strains *in vitro*. We predicted that this shift in fitness cost would result in a more challenging escape path *in vivo*. Consistent with this hypothesis, AAV8-VRC07 administration to $HIV_{REJO.c}$-infected animals harboring mutant Pol resulted in sustained viral suppression.

Fitness landscapes are frequently used to understand HIV evolution, including the dynamics of intrapatient adaptation[83] and antiretroviral escape.[84] Within this framework, it is well known that a fitness cost is typically accrued during escape from cytotoxic T lymphocytes,[85–87] antiretroviral drugs,[88–91] or antibodies.[92] Indeed, modern ART leverages this understanding to maximize their clinical efficacy.[93] Our findings suggest that bNAb escape paths are predictable and that maximizing the cost of escape *in vivo* may be the key to improving their clinical efficacy. Whether analogous improvements in the clinical efficacy of bNAbs could be achieved by reducing the fitness of viruses replicating in patients who have failed ART regimens remains to be determined. Recent efforts focus on antibody combinations that target independent sites of vulnerability; however, future bNAb combinations with orthogonal, high-cost escape paths should be tested, as combinations whose escape mutations result in additive fitness costs may improve the therapeutic efficacy of antibody-based interventions.

Limitations of the study

Despite our best effort to be comprehensive, our study has a number of limitations. First, we reported the results of only three antibodies targeting two distinct sites of vulnerability against two clade B isolates of HIV. However, there are a plethora of bNAbs that target the sites of vulnerability, and many diverse HIV isolates exist.[94] Whether our findings would extend to other bNAbs and HIV clades remains to be determined. However, several reports show that mutations and evolutionary paths are conserved and convergent across different isolates and clades.[95–97] Second, differences in bNAb concentration influenced the resulting escape paths. Future studies could focus on dissecting the influence of bNAb concentration on escape path selection. In addition, AAV-mediated antibody delivery starts with lower serum concentrations of bNAb before achieving a high steady-state concentration, whereas passive transfer results in high initial concentration, which then declines over time. However, our data show that similar escape paths were selected irrespective of the bNAb delivery approach. Third, our study focused on escape mutations present at the endpoint of each independent experiment; therefore, the dynamic events occurring earlier and over the course of escape still need to be elucidated. Fourth, humanized mice have a relatively small blood volume that may not completely recapitulate HIV infection in humans.[98] Moreover, BLT mice elicit a poor humoral immune response and therefore

lack this selective pressure,[99] which may influence the selection of escape paths. In the case of PGDM1400, the polyclonal humoral response elicited in humans is reactive against the various glycans on the Env protein.[100] Viremic patients receiving individual bNAbs exhibit more substantial drops in viral load than what was seen in our model.[34,35,41,69] Additionally, there are reports of synergy between passively transferred bNAbs and endogenous antibody responses in patients,[101] which are unlikely to occur in humanized mice. Despite deficiencies in the endogenous humoral immunity of humanized mice, we found the same VRC07, N6, and PGDM1400 escape mutations seen in NHPs and humans, with the benefit of a shorter time frame and lower cost.[102] Given their diverse and continuously evolving viral population, as previously reported,[31] HIV-infected humanized mice represent an excellent model to evaluate bNAb escape *in vivo*, as they may represent a high bar for therapeutic efficacy, as suppression is completely dependent on the administered bNAb. Finally, measurements of viral growth rates were performed *in vitro* with PBMCs from a single donor. Whether the absolute growth rate of these mutants across genetically distinct patients varies remains untested, but previous studies suggest that their relative fitness would remain unchanged.[65]

RESOURCE AVAILABILITY

Lead contact

Further information and requests for resources and reagents should be directed to and will be fulfilled by the lead contact, Dr. Alejandro B. Balazs (abalazs@mgh.harvard.edu).

Materials availability

All genetic constructs and unique biological materials generated in this study are available from the lead contact without restriction upon request.

Data and code availability

Raw sequencing files reported in this paper were deposited in the NCBI Short Read Archive (SRA) under accession number SRA: PRJNA1399940. All other data are available in the main text or as part of the supplemental data and tables. Codes used for the sequencing analyses in this study along with instructions to run them and a summary of the analyzed sequencing data are available online at Zenodo: https://doi.org/10.5281/zenodo.18187084. Any additional information required to reanalyze the data reported in this paper is available from the lead contact upon request.

ACKNOWLEDGMENTS

We wish to thank Dennis Burton (Scripps) for providing antibody proteins and Dan Barouch for providing anti-PGDM1400 idiotype antibody protein. We also thank K.L. Clayton and D.T. Claiborne for advice on experimental design and the manuscript. We thank the Ragon Institute Protein Core for providing antibody proteins. The following reagents were obtained through the NIH HIV Reagent Program, the Division of AIDS, the NIAID, and the NIH: HIV-1, strain JR-CSF IMC (pYK-JRCSF), and ARP-2708, contributed by Dr. Irvin S.Y. Chen and Dr. Yoshio Koyanagi; ARP-11746 (pREJO.c/2864), contributed by Dr. John Kappes and Dr. Christina Ochsenbauer; and TZM-bl cells and ARP-8129, contributed by Dr. John C. Kappes, Dr. Xiaoyun Wu, and Tranzyme Inc. N.M.S.G. was supported by the Executive Committee on Research (ECOR) of the Mass General Hospital (MGH) Fund for Medical Discovery (FMD) Fundamental Research Fellowship Award. A.D.N. was supported by the Ruth L. Kirschstein National Research Service Award (NRSA) Postdoctoral Training Program award T32AI007245. C.E.D. was supported by the NRSA Individual Postdoctoral Fellowship 1F32AI125096-01A1. J.M.B. was supported by the NSRA Predoctoral Award 1F31AI131747-01A1. A.B.B. was supported by the National Institute for Allergy and Infectious Disease Career Transition award K22AI102769, research grants R01AI174875 and R01AI174276, the National Institutes for Drug Abuse (NIDA) Avenir New Innovator award DP2DA040254, the NIDA Avant-Garde Award 1DP1DA060607, CDC subcontract 200-2016-91773-T.O.2, the MGH Transformative Scholars Program, and funding from the Charles H. Hood Foundation. This independent research was supported by the Gilead Sciences Research Scholars Program in HIV. The graphical abstract was created in BioRender.

AUTHOR CONTRIBUTIONS

C.E.D. and A.B.B. designed the experiments. N.M.S.G., A.D.N., Y.C., C.E.D., C.L.B., S.W.M., Y.E.S.A., E.C.L., M.L.S., D.P., A.Z.L., M.J.D., S.B.Y., B.M., and C.B.B. carried out experiments and analyzed data. J.M.B., A.P., X.C., C.L., R.A.K., J.R.M., and D.L. offered suggestions for experiments and provided key materials. S.T. and V.D.V. provided humanized mice. N.M.S.G., A.D.N., Y.C., C.E.D., and A.B.B. wrote the paper with contributions from all authors. The authors of this study fulfill all the authorship criteria required by Cell Press. Roles and responsibilities were agreed upon among the authors ahead of the research within reason, and changes to these roles were previously agreed upon by the authors.

DECLARATION OF INTERESTS

A.B.B. is a founder of Cure Systems LLC.

STAR★METHODS

Detailed methods are provided in the online version of this paper and include the following:

- KEY RESOURCES TABLE
- EXPERIMENTAL MODEL AND STUDY PARTICIPANT DETAILS
  - Human samples
  - BLT Humanized Mice
  - Cell Lines
- METHOD DETAILS
  - HIV production
  - Humanized mouse HIV infection
  - AAVs vector production, quantification, validation, and administration
  - Antibody quantification by ELISA
  - Viral load test by quantitative RT-PCR (RT-qPCR)
  - Illumina deep sequencing and identification of HIV envelope mutants
  - Envelope Escape Mutant Analysis
  - Viral Diversity and Variant Conservation Analysis
  - Construction of HIV mutants
  - *In vitro* neutralization assay
  - Determination of viral fitness
  - Escape Barrier Analysis
  - Passive transfer experiments
  - *In vivo* antiretroviral selection-pressure of HIV

SUPPLEMENTAL INFORMATION

Supplemental information can be found online at https://doi.org/10.1016/j.immuni.2026.01.031.

Received: July 9, 2025
Revised: January 27, 2026
Accepted: January 29, 2026
Published: February 25, 2026

REFERENCES

1. Landovitz, R.J., Scott, H., and Deeks, S.G. (2023). Prevention, treatment and cure of HIV infection. Nat. Rev. Microbiol. *21*, 657–670. https://doi.org/10.1038/s41579-023-00914-1.

2. Bekker, L.-G., Das, M., Abdool Karim, Q., Ahmed, K., Batting, J., Brumskine, W., Gill, K., Harkoo, I., Jaggernath, M., Kigozi, G., et al. (2024). Twice-Yearly Lenacapavir or Daily F/TAF for HIV Prevention in Cisgender Women. N. Engl. J. Med. *391*, 1179–1192. https://doi.org/10.1056/NEJMoa2407001.

3. Jewell, B.L., Mudimu, E., Stover, J., ten Brink, D., Phillips, A.N., Smith, J.A., Martin-Hughes, R., Teng, Y., Glaubius, R., Mahiane, S.G., et al. (2020). Potential effects of disruption to HIV programmes in sub-Saharan Africa caused by COVID-19: results from multiple mathematical models. Lancet HIV *7*, e629–e640. https://doi.org/10.1016/S2352-3018(20)30211-3.

4. McCoy, L.E., and Burton, D.R. (2017). Identification and specificity of broadly neutralizing antibodies against HIV. Immunol. Rev. *275*, 11–20. https://doi.org/10.1111/imr.12484.

5. Sajadi, M.M., Dashti, A., Rikhtegaran Tehrani, Z., Tolbert, W.D., Seaman, M.S., Ouyang, X., Gohain, N., Pazgier, M., Kim, D., Cavet, G., et al. (2018). Identification of Near-Pan-neutralizing Antibodies against HIV-1 by Deconvolution of Plasma Humoral Responses. Cell *173*, 1783–1795.e14. https://doi.org/10.1016/j.cell.2018.03.061.

6. deCamp, A., Hraber, P., Bailer, R.T., Seaman, M.S., Ochsenbauer, C., Kappes, J., Gottardo, R., Edlefsen, P., Self, S., Tang, H., et al. (2014). Global Panel of HIV-1 Env Reference Strains for Standardized Assessments of Vaccine-Elicited Neutralizing Antibodies. J. Virol. *88*, 2489–2507. https://doi.org/10.1128/JVI.02853-13.

7. Sok, D., and Burton, D.R. (2018). Recent progress in broadly neutralizing antibodies to HIV. Nat. Immunol. *19*, 1179–1188. https://doi.org/10.1038/s41590-018-0235-7.

8. Wu, X., Zhang, Z., Schramm, C.A., Joyce, M.G., Kwon, Y.D., Zhou, T., Sheng, Z., Zhang, B., O'Dell, S., McKee, K., et al. (2015). Maturation and Diversity of the VRC01-Antibody Lineage over 15 Years of Chronic HIV-1 Infection. Cell *161*, 470–485. https://doi.org/10.1016/j.cell.2015.03.004.

9. Diskin, R., Scheid, J.F., Marcovecchio, P.M., West, A.P., Klein, F., Gao, H., Gnanapragasam, P.N.P., Abadir, A., Seaman, M.S., Nussenzweig, M.C., et al. (2011). Increasing the Potency and Breadth of an HIV Antibody by Using Structure-Based Rational Design. Science *334*, 1289–1293. https://doi.org/10.1126/science.1213782.

10. Doria-Rose, N.A., Bhiman, J.N., Roark, R.S., Schramm, C.A., Gorman, J., Chuang, G.-Y., Pancera, M., Cale, E.M., Ernandes, M.J., Louder, M.K., et al. (2016). New Member of the V1V2-Directed CAP256-VRC26 Lineage That Shows Increased Breadth and Exceptional Potency. J. Virol. *90*, 76–91. https://doi.org/10.1128/JVI.01791-15.

11. Balazs, A.B., Ouyang, Y., Hong, C.M., Chen, J., Nguyen, S.M., Rao, D.S., An, D.S., and Baltimore, D. (2014). Vectored immunoprophylaxis protects humanized mice from mucosal HIV transmission. Nat. Med. *20*, 296–300. https://doi.org/10.1038/nm.3471.

12. Balazs, A.B., Chen, J., Hong, C.M., Rao, D.S., Yang, L., and Baltimore, D. (2011). Antibody-based protection against HIV infection by vectored immunoprophylaxis. Nature *481*, 81–84. https://doi.org/10.1038/nature10660.

13. Deruaz, M., Moldt, B., Le, K.M., Power, K.A., Vrbanac, V.D., Tanno, S., Ghebremichael, M.S., Allen, T.M., Tager, A.M., Burton, D.R., et al. (2016). Protection of Humanized Mice From Repeated Intravaginal HIV Challenge by Passive Immunization: A Model for Studying the Efficacy of Neutralizing Antibodies In Vivo. J. Infect. Dis. *214*, 612–616. https://doi.org/10.1093/infdis/jiw203.

14. Stoddart, C.A., Galkina, S.A., Joshi, P., Kosikova, G., Long, B.R., Maidji, E., Moreno, M.E., Rivera, J.M., Sanford, U.R., Sloan, B., et al. (2014). Efficacy of broadly neutralizing monoclonal antibody PG16 in HIV-infected humanized mice. Virology *462–463*, 115–125. https://doi.org/10.1016/j.virol.2014.05.036.

15. Veselinovic, M., Neff, C.P., Mulder, L.R., and Akkina, R. (2012). Topical gel formulation of broadly neutralizing anti-HIV-1 monoclonal antibody VRC01 confers protection against HIV-1 vaginal challenge in a humanized mouse model. Virology *432*, 505–510. https://doi.org/10.1016/j.virol.2012.06.025.

16. Brady, J.M., Phelps, M., MacDonald, S.W., Lam, E.C., Nitido, A., Parsons, D., Boutros, C.L., Deal, C.E., Garcia-Beltran, W.F., Tanno, S., et al. (2022). Antibody-mediated prevention of vaginal HIV transmission is dictated by IgG subclass in humanized mice. Sci. Transl. Med. *14*, eabn9662. https://doi.org/10.1126/scitranslmed.abn9662.

17. Rudicell, R.S., Kwon, Y.D., Ko, S.-Y., Pegu, A., Louder, M.K., Georgiev, I.S., Wu, X., Zhu, J., Boyington, J.C., Chen, X., et al. (2014). Enhanced potency of a broadly neutralizing HIV-1 antibody in vitro improves protection against lentiviral infection in vivo. J. Virol. *88*, 12669–12682. https://doi.org/10.1128/JVI.02213-14.

18. Julg, B., Liu, P.-T., Wagh, K., Fischer, W.M., Abbink, P., Mercado, N.B., Whitney, J.B., Nkolola, J.P., McMahan, K., Tartaglia, L.J., et al. (2017). Protection against a mixed SHIV challenge by a broadly neutralizing antibody cocktail. Sci. Transl. Med. *9*, eaao4235. https://doi.org/10.1126/scitranslmed.aao4235.

19. Julg, B., Tartaglia, L.J., Keele, B.F., Wagh, K., Pegu, A., Sok, D., Abbink, P., Schmidt, S.D., Wang, K., Chen, X., et al. (2017). Broadly neutralizing antibodies targeting the HIV-1 envelope V2 apex confer protection against a clade C SHIV challenge. Sci. Transl. Med. *9*, eaal1321. https://doi.org/10.1126/scitranslmed.aal1321.

20. Julg, B., Sok, D., Schmidt, S.D., Abbink, P., Newman, R.M., Broge, T., Linde, C., Nkolola, J., Le, K., Su, D., et al. (2017). Protective Efficacy of Broadly Neutralizing Antibodies with Incomplete Neutralization Activity against Simian-Human Immunodeficiency Virus in Rhesus Monkeys. J. Virol. *91*, e01187-17. https://doi.org/10.1128/JVI.01187-17.

21. Moldt, B., Rakasz, E.G., Schultz, N., Chan-Hui, P.-Y., Swiderek, K., Weisgrau, K.L., Piaskowski, S.M., Bergman, Z., Watkins, D.I., Poignard, P., et al. (2012). Highly potent HIV-specific antibody neutralization in vitro translates into effective protection against mucosal SHIV challenge in vivo. Proc. Natl. Acad. Sci. USA *109*, 18921–18925. https://doi.org/10.1073/pnas.1214785109.

22. Corey, L., Gilbert, P.B., Juraska, M., Montefiori, D.C., Morris, L., Karuna, S.T., Edupuganti, S., Mgodi, N.M., deCamp, A.C., Rudnicki, E., et al. (2021). Two Randomized Trials of Neutralizing Antibodies to Prevent HIV-1 Acquisition. N. Engl. J. Med. *384*, 1003–1014. https://doi.org/10.1056/NEJMoa2031738.

23. Mayer, K.H., Seaton, K.E., Huang, Y., Grunenberg, N., Isaacs, A., Allen, M., Ledgerwood, J.E., Frank, I., Sobieszczyk, M.E., Baden, L.R., et al. (2017). Safety, pharmacokinetics, and immunological activities of multiple intravenous or subcutaneous doses of an anti-HIV monoclonal antibody, VRC01, administered to HIV-uninfected adults: Results of a phase 1 randomized trial. PLoS Med. *14*, e1002435. https://doi.org/10.1371/journal.pmed.1002435.

24. Gilbert, P.B., Huang, Y., deCamp, A.C., Karuna, S., Zhang, Y., Magaret, C.A., Giorgi, E.E., Korber, B., Edlefsen, P.T., Rossenkhan, R., et al. (2022). Neutralization titer biomarker for antibody-mediated prevention of HIV-1 acquisition. Nat. Med. *28*, 1924–1932. https://doi.org/10.1038/s41591-022-01953-6.

25. Badamchi-Zadeh, A., Tartaglia, L.J., Abbink, P., Bricault, C.A., Liu, P.-T., Boyd, M., Kirilova, M., Mercado, N.B., Nanayakkara, O.S., Vrbanac, V.D., et al. (2018). Therapeutic Efficacy of Vectored PGT121 Gene Delivery in HIV-1-Infected Humanized Mice. J. Virol. *92*, e01925-17. https://doi.org/10.1128/JVI.01925-17.

26. Barouch, D.H., Whitney, J.B., Moldt, B., Klein, F., Oliveira, T.Y., Liu, J., Stephenson, K.E., Chang, H.-W., Shekhar, K., Gupta, S., et al. (2013). Therapeutic efficacy of potent neutralizing HIV-1-specific monoclonal antibodies in SHIV-infected rhesus monkeys. Nature *503*, 224–228. https://doi.org/10.1038/nature12744.

27. Borducchi, E.N., Liu, J., Nkolola, J.P., Cadena, A.M., Yu, W.-H., Fischinger, S., Broge, T., Abbink, P., Mercado, N.B., Chandrashekar, A., et al. (2018). Antibody and TLR7 agonist delay viral rebound in SHIV-infected monkeys. Nature *563*, 360–364. https://doi.org/10.1038/s41586-018-0600-6.

28. Halper-Stromberg, A., Lu, C.-L., Klein, F., Horwitz, J.A., Bournazos, S., Nogueira, L., Eisenreich, T.R., Liu, C., Gazumyan, A., Schaefer, U., et al. (2014). Broadly Neutralizing Antibodies and Viral Inducers Decrease Rebound from HIV-1 Latent Reservoirs in Humanized Mice. Cell *158*, 989–999. https://doi.org/10.1016/j.cell.2014.07.043.

29. Horwitz, J.A., Halper-Stromberg, A., Mouquet, H., Gitlin, A.D., Tretiakova, A., Eisenreich, T.R., Malbec, M., Gravemann, S., Billerbeck, E., Dorner, M., et al. (2013). HIV-1 suppression and durable control by combining single broadly neutralizing antibodies and antiretroviral drugs in humanized mice. Proc. Natl. Acad. Sci. USA. *110*, 16538–16543. https://doi.org/10.1073/pnas.1315295110.

30. Julg, B., Pegu, A., Abbink, P., Liu, J., Brinkman, A., Molloy, K., Mojta, S., Chandrashekar, A., Callow, K., Wang, K., et al. (2017). Virological Control by the CD4-Binding Site Antibody N6 in Simian-Human Immunodeficiency Virus-Infected Rhesus Monkeys. J. Virol. *91*, e00498-17. https://doi.org/10.1128/JVI.00498-17.

31. Klein, F., Halper-Stromberg, A., Horwitz, J.A., Gruell, H., Scheid, J.F., Bournazos, S., Mouquet, H., Spatz, L.A., Diskin, R., Abadir, A., et al. (2012). HIV therapy by a combination of broadly neutralizing antibodies in humanized mice. Nature *492*, 118–122. https://doi.org/10.1038/nature11604.

32. Shingai, M., Nishimura, Y., Klein, F., Mouquet, H., Donau, O.K., Plishka, R., Buckler-White, A., Seaman, M., Piatak, M., Lifson, J.D., et al. (2013). Antibody-mediated immunotherapy of macaques chronically infected with SHIV suppresses viraemia. Nature *503*, 277–280. https://doi.org/10.1038/nature12746.

33. Bar, K.J., Sneller, M.C., Harrison, L.J., Justement, J.S., Overton, E.T., Petrone, M.E., Salantes, D.B., Seamon, C.A., Scheinfeld, B., Kwan, R.W., et al. (2016). Effect of HIV Antibody VRC01 on Viral Rebound after Treatment Interruption. N. Engl. J. Med. *375*, 2037–2050. https://doi.org/10.1056/NEJMoa1608243.

34. Caskey, M., Klein, F., Lorenzi, J.C.C., Seaman, M.S., West, A.P., Buckley, N., Kremer, G., Nogueira, L., Braunschweig, M., Scheid, J.F., et al. (2015). Viraemia suppressed in HIV-1-infected humans by broadly neutralizing antibody 3BNC117. Nature *522*, 487–491. https://doi.org/10.1038/nature14411.

35. Caskey, M., Schoofs, T., Gruell, H., Settler, A., Karagounis, T., Kreider, E.F., Murrell, B., Pfeifer, N., Nogueira, L., Oliveira, T.Y., et al. (2017). Antibody 10–1074 suppresses viremia in HIV-1-infected individuals. Nat. Med. *23*, 185–191. https://doi.org/10.1038/nm.4268.

36. Lynch, R.M., Wong, P., Tran, L., O'Dell, S., Nason, M.C., Li, Y., Wu, X., and Mascola, J.R. (2015). HIV-1 fitness cost associated with escape from the VRC01 class of CD4 binding site neutralizing antibodies. J. Virol. *89*, 4201–4213. https://doi.org/10.1128/JVI.03608-14.

37. Mehandru, S., Vcelar, B., Wrin, T., Stiegler, G., Joos, B., Mohri, H., Boden, D., Galovich, J., Tenner-Racz, K., Racz, P., et al. (2007). Adjunctive passive immunotherapy in human immunodeficiency virus type 1-infected individuals treated with antiviral therapy during acute and early infection. J. Virol. *81*, 11016–11031. https://doi.org/10.1128/JVI.01340-07.

38. Mendoza, P., Gruell, H., Nogueira, L., Pai, J.A., Butler, A.L., Millard, K., Lehmann, C., Suárez, I., Oliveira, T.Y., Lorenzi, J.C.C., et al. (2018). Combination therapy with anti-HIV-1 antibodies maintains viral suppression. Nature *561*, 479–484. https://doi.org/10.1038/s41586-018-0531-2.

39. Trkola, A., Kuster, H., Rusert, P., Joos, B., Fischer, M., Leemann, C., Manrique, A., Huber, M., Rehr, M., Oxenius, A., et al. (2005). Delay of HIV-1 rebound after cessation of antiretroviral therapy through passive transfer of human neutralizing antibodies. Nat. Med. *11*, 615–622. https://doi.org/10.1038/nm1244.

40. Happe, M., Lynch, R.M., Fichtenbaum, C.J., Heath, S.L., Koletar, S.L., Landovitz, R.J., Presti, R.M., Santana-Bagur, J.L., Tressler, R.L., Holman, L.A., et al. (2025). Virologic effects of broadly neutralizing antibodies VRC01LS and VRC07-523LS on chronic HIV-1 infection. JCI Insight *10*, e181496. https://doi.org/10.1172/jci.insight.181496.

41. Bar-On, Y., Gruell, H., Schoofs, T., Pai, J.A., Nogueira, L., Butler, A.L., Millard, K., Lehmann, C., Rez, I.S., Oliveira, T.Y., et al. (2018). Safety and antiviral activity of combination HIV-1 broadly neutralizing antibodies in viremic individuals. Nat. Med. *24*, 1–13. https://doi.org/10.1038/s41591-018-0186-4.

42. Julg, B., Walker-Sperling, V.E.K., Wagh, K., Aid, M., Stephenson, K.E., Zash, R., Liu, J., Nkolola, J.P., Hoyt, A., Castro, M., et al. (2024). Safety and antiviral effect of a triple combination of HIV-1 broadly neutralizing antibodies: a phase 1/2a trial. Nat. Med. *30*, 3534–3543. https://doi.org/10.1038/s41591-024-03247-5.

43. Ledgerwood, J.E., Coates, E.E., Yamshchikov, G., Saunders, J.G., Holman, L., Enama, M.E., DeZure, A., Lynch, R.M., Gordon, I., Plummer, S., et al. (2015). Safety, Pharmacokinetics and Neutralization of the Broadly Neutralizing HIV-1 Human Monoclonal Antibody VRC01 in Healthy Adults. Clin. Exp. Immunol. *182*, 289–301. https://doi.org/10.1111/cei.12692.

44. Lewis, A.D., Chen, R., Montefiori, D.C., Johnson, P.R., and Clark, K.R. (2002). Generation of Neutralizing Activity against Human Immunodeficiency Virus Type 1 in Serum by Antibody Gene Transfer. J. Virol. *76*, 8769–8775. https://doi.org/10.1128/JVI.76.17.8769-8775.2002.

45. Fang, J., Qian, J.-J., Yi, S., Harding, T.C., Tu, G.H., VanRoey, M., and Jooss, K. (2005). Stable antibody expression at therapeutic levels using the 2A peptide. Nat. Biotechnol. *23*, 584–590. https://doi.org/10.1038/nbt1087.

46. Fuchs, S.P., Martinez-Navio, J.M., Piatak, M., Lifson, J.D., Gao, G., and Desrosiers, R.C. (2015). AAV-Delivered Antibody Mediates Significant Protective Effects against SIVmac239 Challenge in the Absence of Neutralizing Activity. PLoS Pathog. *11*, e1005090. https://doi.org/10.1371/journal.ppat.1005090.

47. Gardner, M.R., Kattenhorn, L.M., Kondur, H.R., von Schaewen, M., Dorfman, T., Chiang, J.J., Haworth, K.G., Decker, J.M., Alpert, M.D., Bailey, C.C., et al. (2015). AAV-expressed eCD4-Ig provides durable protection from multiple SHIV challenges. Nature *519*, 87–91. https://doi.org/10.1038/nature14264.

48. Brady, J.M., Baltimore, D., and Balazs, A.B. (2017). Antibody gene transfer with adeno-associated viral vectors as a method for HIV prevention. Immunol. Rev. *275*, 324–333. https://doi.org/10.1111/imr.12478.

49. Saunders, K.O., Wang, L., Joyce, M.G., Yang, Z.-Y., Balazs, A.B., Cheng, C., Ko, S.-Y., Kong, W.-P., Rudicell, R.S., Georgiev, I.S., et al. (2015). Broadly Neutralizing Human Immunodeficiency Virus Type 1 Antibody Gene Transfer Protects Nonhuman Primates from Mucosal Simian-Human Immunodeficiency Virus Infection. J. Virol. *89*, 8334–8345. https://doi.org/10.1128/JVI.00908-15.

50. Welles, H.C., Jennewein, M.F., Mason, R.D., Narpala, S., Wang, L., Cheng, C., Zhang, Y., Todd, J.-P., Lifson, J.D., Balazs, A.B., et al. (2018). Vectored delivery of anti-SIV envelope targeting mAb via AAV8 protects rhesus macaques from repeated limiting dose intrarectal swarm SIVsmE660 challenge. PLoS Pathog. *14*, e1007395. https://doi.org/10.1371/journal.ppat.1007395.

51. Casazza, J.P., Cale, E.M., Narpala, S., Yamshchikov, G.V., Coates, E.E., Hendel, C.S., Novik, L., Holman, L.A., Widge, A.T., Apte, P., et al. (2022). Safety and tolerability of AAV8 delivery of a broadly neutralizing antibody in adults living with HIV: a phase 1, dose-escalation trial. Nat. Med. *28*, 1022–1030. https://doi.org/10.1038/s41591-022-01762-x.

52. Fuchs, S.P., Mondragon, P.G., Zabizhin, R., Tomer, S., Wang, L., Cook, E., Dudley, D.M., Weisgrau, K.L., Furlott, J., Coonen, J., et al. (2025). Transient rapamycin treatment avoids unwanted host immune responses toward AAV-delivered anti-HIV antibodies. Nat. Commun. *16*, 8906. https://doi.org/10.1038/s41467-025-63970-6.

53. Ardeshir, A., O'Hagan, D., Mehta, I., Shandilya, S., Hopkins, L.L.J., Adamson, L., Kuroda, M.J., Hahn, P.A., da Costa, L.A.B., Fuchs, S.P., et al. (2025). Determinants of successful AAV-vectored delivery of HIV-1 bNAbs in early life. Nature *645*, 1020–1028. https://doi.org/10.1038/s41586-025-09330-2.

54. Thavarajah, J.J., Hønge, B.L., and Wejse, C.M. (2024). The Use of Broadly Neutralizing Antibodies (bNAbs) in HIV-1 Treatment and Prevention. Viruses *16*, 911. https://doi.org/10.3390/v16060911.

55. Koyanagi, Y., Miles, S., Mitsuyasu, R.T., Merrill, J.E., Vinters, H.V., and Chen, I.S. (1987). Dual infection of the central nervous system by AIDS viruses with distinct cellular tropisms. Science *236*, 819–822. https://doi.org/10.1126/science.3646751.

56. Ochsenbauer, C., Edmonds, T.G., Ding, H., Keele, B.F., Decker, J., Salazar, M.G., Salazar-Gonzalez, J.F., Shattock, R., Haynes, B.F., Shaw, G.M., et al. (2012). Generation of Transmitted/Founder HIV-1 Infectious Molecular Clones and Characterization of Their Replication Capacity in CD4 T Lymphocytes and Monocyte-Derived Macrophages. J. Virol. *86*, 2715–2728. https://doi.org/10.1128/JVI.06157-11.

57. McCarthy, M., He, J., and Wood, C. (1998). HIV-1 Strain-Associated Variability in Infection of Primary Neuroglia. J. Neurovirol. *4*, 80–89. https://doi.org/10.3109/13550289809113484.

58. Charlesworth, D., Barton, N.H., and Charlesworth, B. (2017). The sources of adaptive variation. Proc. Biol. Sci. *284*, 20162864. https://doi.org/10.1098/rspb.2016.2864.

59. Baenziger, S., Tussiwand, R., Schlaepfer, E., Mazzucchelli, L., Heikenwalder, M., Kurrer, M.O., Behnke, S., Frey, J., Oxenius, A., Joller, H., et al. (2006). Disseminated and sustained HIV infection in CD34+ cord blood cell-transplanted Rag2-/-gamma c-/- mice. Proc. Natl. Acad. Sci. USA *103*, 15951–15956. https://doi.org/10.1073/pnas.0604493103.

60. Sun, Z., Denton, P.W., Estes, J.D., Othieno, F.A., Wei, B.L., Wege, A.K., Melkus, M.W., Padgett-Thomas, A., Zupancic, M., Haase, A.T., et al. (2007). Intrarectal transmission, systemic infection, and CD4+ T cell depletion in humanized mice infected with HIV-1. J. Exp. Med. *204*, 705–714. https://doi.org/10.1084/jem.20062411.

61. Melkus, M.W., Estes, J.D., Padgett-Thomas, A., Gatlin, J., Denton, P.W., Othieno, F.A., Wege, A.K., Haase, A.T., and Garcia, J.V. (2006). Humanized mice mount specific adaptive and innate immune responses to EBV and TSST-1. Nat. Med. *12*, 1316–1322. https://doi.org/10.1038/nm1431.

62. Huang, J., Kang, B.H., Ishida, E., Zhou, T., Griesman, T., Sheng, Z., Wu, F., Doria-Rose, N.A., Zhang, B., McKee, K., et al. (2016). Identification of a CD4-Binding Site Antibody to HIV that Evolved Near-Pan Neutralization Breadth. Immunity *45*, 1108–1121. https://doi.org/10.1016/j.immuni.2016.10.027.

63. Sok, D., van Gils, M.J., Pauthner, M., Julien, J.-P., Saye-Francisco, K.L., Hsueh, J., Briney, B., Lee, J.H., Le, K.M., Lee, P.S., et al. (2014). Recombinant HIV envelope trimer selects for quaternary-dependent antibodies targeting the trimer apex. Proc. Natl. Acad. Sci. USA *111*, 17624–17629. https://doi.org/10.1073/pnas.1415789111.

64. Webb, N.E., Montefiori, D.C., and Lee, B. (2015). Dose–response curve slope helps predict therapeutic potency and breadth of HIV broadly neutralizing antibodies. Nat. Commun. *6*, 8443. https://doi.org/10.1038/ncomms9443.

65. Galvez, N.M.S., Sheehan, M.L., Lin, A.Z., Cao, Y., Lam, E.C., Jackson, A.M., and Balazs, A.B. (2024). QuickFit: A High-Throughput RT-qPCR-Based Assay to Quantify Viral Growth and Fitness In Vitro. Viruses *16*, 1320. https://doi.org/10.3390/v16081320.

66. Wainberg, M.A. (2004). The impact of the M184V substitution on drug resistance and viral fitness. Expert Rev. Anti-infect. Ther. *2*, 147–151. https://doi.org/10.1586/14787210.2.1.147.

67. Julg, B., Stephenson, K.E., Wagh, K., Tan, S.C., Zash, R., Walsh, S., Ansel, J., Kanjilal, D., Nkolola, J., Walker-Sperling, V.E.K., et al. (2022). Safety and antiviral activity of triple combination broadly neutralizing monoclonal antibody therapy against HIV-1: a phase 1 clinical trial. Nat. Med. *28*, 1288–1296. https://doi.org/10.1038/s41591-022-01815-1.

68. Pegu, A., Xu, L., DeMouth, M.E., Fabozzi, G., March, K., Almasri, C.G., Cully, M.D., Wang, K., Yang, E.S., Dias, J., et al. (2022). Potent anti-viral activity of a trispecific HIV neutralizing antibody in SHIV-infected monkeys. Cell Rep. *38*, 110199. https://doi.org/10.1016/j.celrep.2021.110199.

69. Lynch, R.M., Boritz, E., Coates, E.E., DeZure, A., Madden, P., Costner, P., Enama, M.E., Plummer, S., Holman, L., Hendel, C.S., et al. (2015). Virologic effects of broadly neutralizing antibody VRC01 administration during chronic HIV-1 infection. Sci. Transl. Med. *7*, 319ra206. https://doi.org/10.1126/scitranslmed.aad5752.

70. Schoofs, T., Klein, F., Braunschweig, M., Kreider, E.F., Feldmann, A., Nogueira, L., Oliveira, T., Lorenzi, J.C.C., Parrish, E.H., Learn, G.H., et al. (2016). HIV-1 therapy with monoclonal antibody 3BNC117 elicits host immune responses against HIV-1. Science *352*, 997–1001. https://doi.org/10.1126/science.aaf0972.

71. Scheid, J.F., Horwitz, J.A., Bar-On, Y., Kreider, E.F., Lu, C.-L., Lorenzi, J.C.C., Feldmann, A., Braunschweig, M., Nogueira, L., Oliveira, T., et al. (2016). HIV-1 antibody 3BNC117 suppresses viral rebound in humans during treatment interruption. Nature *535*, 556–560. https://doi.org/10.1038/nature18929.

72. Otsuka, Y., Schmitt, K., Quinlan, B.D., Gardner, M.R., Alfant, B., Reich, A., Farzan, M., and Choe, H. (2018). Diverse pathways of escape from all well-characterized VRC01-class broadly neutralizing HIV-1 antibodies. PLoS Pathog. *14*, e1007238. https://doi.org/10.1371/journal.ppat.1007238.

73. Wise, M.C., Xu, Z., Tello-Ruiz, E., Beck, C., Trautz, A., Patel, A., Elliott, S.T.C., Chokkalingam, N., Kim, S., Kerkau, M.G., et al. (2020). In vivo delivery of synthetic DNA–encoded antibodies induces broad HIV-1–neutralizing activity. J. Clin. Investig. *130*, 827–837. https://doi.org/10.1172/JCI132779.

74. Wu, R.L., Houser, K.V., Gaudinski, M.R., Widge, A.T., Awan, S.F., Carter, C.A., Holman, L.A., Saunders, J., Hendel, C.S., Eshun, A., et al. (2025). Safety and pharmacokinetics of N6LS, a broadly neutralising monoclonal antibody for HIV: a phase 1, open-label, dose-escalation study in healthy adults. Lancet HIV *12*, e485–e495. https://doi.org/10.1016/s2352-3018(25)00041-4.

75. Moore, P.L., Gray, E.S., Sheward, D., Madiga, M., Ranchobe, N., Lai, Z., Honnen, W.J., Nonyane, M., Tumba, N., Hermanus, T., et al. (2011). Potent and broad neutralization of HIV-1 subtype C by plasma antibodies targeting a quaternary epitope including residues in the V2 loop. J. Virol. *85*, 3128–3141. https://doi.org/10.1128/JVI.02658-10.

76. Radford, C.E., and Bloom, J.D. (2025). Comprehensive maps of escape mutations from antibodies 10-1074 and 3BNC117 for Envs from two divergent HIV strains. J. Virol. *99*, e0019525. https://doi.org/10.1128/jvi.00195-25.

77. Neher, R.A., and Leitner, T. (2010). Recombination Rate and Selection Strength in HIV Intra-patient Evolution. PLoS Comput. Biol. *6*, e1000660. https://doi.org/10.1371/journal.pcbi.1000660.

78. Li, Y., O'Dell, S., Walker, L.M., Wu, X., Guenaga, J., Feng, Y., Schmidt, S.D., McKee, K., Louder, M.K., Ledgerwood, J.E., et al. (2011). Mechanism of neutralization by the broadly neutralizing HIV-1 monoclonal antibody VRC01. J. Virol. *85*, 8954–8967. https://doi.org/10.1128/JVI.00754-11.

79. Pegu, A., Borate, B., Huang, Y., Pauthner, M.G., Hessell, A.J., Julg, B., Doria-Rose, N.A., Schmidt, S.D., Carpp, L.N., Cully, M.D., et al. (2019). A Meta-analysis of Passive Immunization Studies Shows that Serum-Neutralizing Antibody Titer Associates with Protection against SHIV Challenge. Cell Host Microbe *26*, 336–346.e3. https://doi.org/10.1016/j.chom.2019.08.014.

80. Fellinger, C.H., Gardner, M.R., Weber, J.A., Alfant, B., Zhou, A.S., and Farzan, M. (2019). eCD4-Ig limits HIV-1 escape more effectively than CD4-Ig or a broadly neutralizing antibody. J. Virol. *93*, e00443-19. https://doi.org/10.1128/JVI.00443-19.

81. Bricault, C.A., Yusim, K., Seaman, M.S., Yoon, H., Theiler, J., Giorgi, E.E., Wagh, K., Theiler, M., Hraber, P., Macke, J.P., et al. (2019). HIV-1 Neutralizing Antibody Signatures and Application to Epitope-Targeted Vaccine Design. Cell Host Microbe *25*, 59–72.e8. https://doi.org/10.1016/j.chom.2018.12.001.

82. Asmal, M., Luedemann, C., Lavine, C.L., Mach, L.V., Balachandran, H., Brinkley, C., Denny, T.N., Lewis, M.G., Anderson, H., Pal, R., et al.

(2015). Infection of monkeys by simian-human immunodeficiency viruses with transmitted/founder clade C HIV-1 envelopes. Virology *475*, 37–45. https://doi.org/10.1016/j.virol.2014.10.032.

83. Wodarz, D., and Nowak, M.A. (1998). The effect of different immune responses on the evolution of virulent CXCR4–tropic HIV. Proc. Biol. Sci. *265*, 2149–2158. https://doi.org/10.1098/rspb.1998.0552.

84. Theys, K., Deforche, K., Beheydt, G., Moreau, Y., Van Laethem, K., Lemey, P., Camacho, R.J., Rhee, S.-Y., Shafer, R.W., Van Wijngaerden, E., et al. (2010). Estimating the individualized HIV-1 genetic barrier to resistance using a nelfinavir fitness landscape. BMC Bioinform. *11*, 409. https://doi.org/10.1186/1471-2105-11-409.

85. Ganusov, V.V., and De Boer, R.J. (2006). Estimating Costs and Benefits of CTL Escape Mutations in SIV/HIV Infection. PLoS Comput. Biol. *2*, e24. https://doi.org/10.1371/journal.pcbi.0020024.

86. Read, E.L., Tovo-Dwyer, A.A., and Chakraborty, A.K. (2012). Stochastic effects are important in intrahost HIV evolution even when viral loads are high. Proc. Natl. Acad. Sci. USA *109*, 19727–19732. https://doi.org/10.1073/pnas.1206940109.

87. Batorsky, R., Sergeev, R.A., and Rouzine, I.M. (2014). The Route of HIV Escape from Immune Response Targeting Multiple Sites Is Determined by the Cost-Benefit Tradeoff of Escape Mutations. PLoS Comput. Biol. *10*, e1003878. https://doi.org/10.1371/journal.pcbi.1003878.

88. Gardner, E.M., Burman, W.J., Steiner, J.F., Anderson, P.L., and Bangsberg, D.R. (2009). Antiretroviral medication adherence and the development of class-specific antiretroviral resistance. AIDS *23*, 1035–1046. https://doi.org/10.1097/QAD.0b013e32832ba8ec.

89. Armstrong, K.L., Lee, T.-H., and Essex, M. (2011). Replicative Fitness Costs of Nonnucleoside Reverse Transcriptase Inhibitor Drug Resistance Mutations on HIV Subtype C. Antimicrob. Agents Chemother. *55*, 2146–2153. https://doi.org/10.1128/AAC.01505-10.

90. Hill, A.L., Rosenbloom, D.I.S., and Nowak, M.A. (2012). Evolutionary dynamics of HIV at multiple spatial and temporal scales. J. Mol. Med. (Berl) *90*, 543–561. https://doi.org/10.1007/s00109-012-0892-1.

91. Zanini, F., Puller, V., Brodin, J., Albert, J., and Neher, R.A. (2017). *In vivo* mutation rates and the landscape of fitness costs of HIV-1. Virus Evol. *3*, vex003. https://doi.org/10.1093/ve/vex003.

92. Meijers, M., Vanshylla, K., Gruell, H., Klein, F., and Lässig, M. (2021). Predicting in vivo escape dynamics of HIV-1 from a broadly neutralizing antibody. Proc. Natl. Acad. Sci. USA *118*, e2104651118. https://doi.org/10.1073/pnas.2104651118.

93. Cong, M.E., Heneine, W., and García-Lerma, J.G. (2007). The Fitness Cost of Mutations Associated with Human Immunodeficiency Virus Type 1 Drug Resistance Is Modulated by Mutational Interactions. J. Virol. *81*, 3037–3041. https://doi.org/10.1128/jvi.02712-06.

94. Caskey, M. (2020). Broadly neutralizing antibodies for the treatment and prevention of HIV infection. Curr. Opin. HIV AIDS *15*, 49–55. https://doi.org/10.1097/COH.0000000000000600.

95. Han, C., Johnson, J., Dong, R., Kandula, R., Kort, A., Wong, M., Yang, T., Breheny, P.J., Brown, G.D., and Haim, H. (2020). Key Positions of HIV-1 Env and Signatures of Vaccine Efficacy Show Gradual Reduction of Population Founder Effects at the Clade and Regional Levels. mBio *11*, e00126-20. https://doi.org/10.1128/mBio.00126-20.

96. Haddox, H.K., Dingens, A.S., Hilton, S.K., Overbaugh, J., and Bloom, J.D. (2018). Mapping mutational effects along the evolutionary landscape of HIV envelope. eLife *7*, e34420. https://doi.org/10.7554/eLife.34420.

97. DeLeon, O., Hodis, H., O'Malley, Y., Johnson, J., Salimi, H., Zhai, Y., Winter, E., Remec, C., Eichelberger, N., Van Cleave, B., et al. (2017). Accurate predictions of population-level changes in sequence and structural properties of HIV-1 Env using a volatility-controlled diffusion model. PLoS Biol. *15*, e2001549. https://doi.org/10.1371/journal.pbio.2001549.

98. Karpel, M.E., Boutwell, C.L., and Allen, T.M. (2015). BLT humanized mice as a small animal model of HIV infection. Curr. Opin. Virol. *13*, 75–80. https://doi.org/10.1016/j.coviro.2015.05.002.

99. Seung, E., and Tager, A.M. (2013). Humoral immunity in humanized mice: a work in progress. J. Infect. Dis. *208*, S155–S159. https://doi.org/10.1093/infdis/jit448.

100. McCoy, L.E., van Gils, M.J., Ozorowski, G., Messmer, T., Briney, B., Voss, J.E., Kulp, D.W., Macauley, M.S., Sok, D., Pauthner, M., et al. (2016). Holes in the Glycan Shield of the Native HIV Envelope Are a Target of Trimer-Elicited Neutralizing Antibodies. Cell Rep. *16*, 2327–2338. https://doi.org/10.1016/j.celrep.2016.07.074.

101. Freund, N.T., Wang, H., Scharf, L., Nogueira, L., Horwitz, J.A., Bar-On, Y., Golijanin, J., Sievers, S.A., Sok, D., Cai, H., et al. (2017). Coexistence of potent HIV-1 broadly neutralizing antibodies and antibody-sensitive viruses in a viremic controller. Sci. Transl. Med. *9*, eaal2144. https://doi.org/10.1126/scitranslmed.aal2144.

102. Zhang, C., Zaman, L.A., Poluektova, L.Y., Gorantla, S., Gendelman, H.E., and Dash, P.K. (2023). Humanized Mice for Studies of HIV-1 Persistence and Elimination. Pathogens *12*, 879. https://doi.org/10.3390/pathogens12070879.

103. Ramakrishnan, M.A. (2016). Determination of 50% endpoint titer using a simple formula. World J. Virol. *5*, 85–86. https://doi.org/10.5501/wjv.v5.i2.85.

104. Chen, S., Zhou, Y., Chen, Y., and Gu, J. (2018). fastp: an ultra-fast all-in-one FASTQ preprocessor. Bioinformatics *34*, i884–i890. https://doi.org/10.1093/bioinformatics/bty560.

105. Langmead, B., and Salzberg, S.L. (2012). Fast gapped-read alignment with Bowtie 2. Nat. Methods *9*, 357–359. https://doi.org/10.1038/nmeth.1923.

106. Li, H., Handsaker, B., Wysoker, A., Fennell, T., Ruan, J., Homer, N., Marth, G., Abecasis, G., and Durbin, R.; 1000 Genome Project Data Processing Subgroup (2009). The Sequence Alignment/Map format and SAMtools. Bioinformatics *25*, 2078–2079. https://doi.org/10.1093/bioinformatics/btp352.

107. Korber, B.T., Foley, B.T., Kuiken, C.L., Pillai, S.K., and Sodroski, J.G. (2014). Numbering Positions in HIV Relative to HXB2CG. LANL. https://www.hiv.lanl.gov/content/sequence/HIV/REVIEWS/HXB2.html.

108. Köster, J., and Rahmann, S. (2012). Snakemake–a scalable bioinformatics workflow engine. Bioinformatics *28*, 2520–2522. https://doi.org/10.1093/bioinformatics/bts480.

109. Wilm, A., Aw, P.P.K., Bertrand, D., Yeo, G.H.T., Ong, S.H., Wong, C.H., Khor, C.C., Petric, R., Hibberd, M.L., and Nagarajan, N. (2012). LoFreq: a sequence-quality aware, ultra-sensitive variant caller for uncovering cell-population heterogeneity from high-throughput sequencing datasets. Nucleic Acids Res. *40*, 11189–11201. https://doi.org/10.1093/nar/gks918.

110. Piantadosi, A., Freije, C.A., Gosmann, C., Ye, S., Park, D., Schaffner, S.F., Tully, D.C., Allen, T.M., Dong, K.L., Sabeti, P.C., et al. (2019). Metagenomic Sequencing of HIV-1 in the Blood and Female Genital Tract Reveals Little Quasispecies Diversity during Acute Infection. J. Virol. *93*, e00804-18. https://doi.org/10.1128/JVI.00804-18.

111. McCrone, J.T., and Lauring, A.S. (2016). Measurements of Intrahost Viral Diversity Are Extremely Sensitive to Systematic Errors in Variant Calling. J. Virol. *90*, 6884–6895. https://doi.org/10.1128/JVI.00667-16.

112. Siebring-van Olst, E., Vermeulen, C., de Menezes, R.X., Howell, M., Smit, E.F., and van Beusechem, V.W. (2013). Affordable Luciferase Reporter Assay for Cell-Based High-Throughput Screening. J. Biomol. Screen. *18*, 453–461. https://doi.org/10.1177/1087057112465184.

113. Borchers, H.W. (2023). Pracma: Practical Numerical Math Functions. Version R Package Version 2.4.4.

114. R Core Team (2024). R: A Language and Environment for Statistical Computing (R Foundation for Statistical Computing).

115. Reagan-Shaw, S., Nihal, M., and Ahmad, N. (2008). Dose translation from animal to human studies revisited. FASEB J. *22*, 659–661. https://doi.org/10.1096/fj.07-9574LSF.

STAR★METHODS

KEY RESOURCES TABLE

REAGENT or RESOURCE	SOURCE	IDENTIFIER
Antibodies		
Anti-Human CD34 Antibody PE	BioLegend	Cat#343606; RRID: AB_1732008
Anti-human CD3 Brilliant Violet 421™	BioLegend	Cat#300434; RRID:AB_10962690
Anti-human CD4 Antibody Brilliant Violet 570™	BioLegend	Cat#300534; RRID: AB_2563791
Anti-human CD8 Brilliant Violet 785™	BioLegend	Cat#300554; RRID: AB_2564382
HIV-1 core antigen-RD1 (PE-conjugated)	Beckman Coulter	Cat#6604667; RRID: AB_1575989
HRP-conjugated goat anti-human IgG-Fc antibody	Bethyl	Cat#A80-104A; RRID: AB_67064
Ultra-LEAF™ Purified anti-human CD28	BioLegend	Cat#302934; RRID: AB_11148949
Ultra-LEAF™ Purified anti-human CD3	BioLegend	Cat#317326; RRID: AB_11150592
Biological Samples		
BLT donor samples	Human Immune System Mouse Program at the Ragon Institute of MGH, MIT, and Harvard	N/A
Frozen Human PBMCs	Allcells	Cat#PB004F; Lot #A2857.
Bacterial and Virus Strains		
SURE 2 SuperCompetent cells	Agilent	Cat#200152
DH5a E. coli cells	Zymo	Cat#T3009
Chemicals, Peptides, and Recombinant Proteins		
Phosphate buffered saline (PBS)	Corning	Cat#21-031-CV
Tris-buffered saline (TBS)	Thermo Scientific	Cat#AAJ75892AE
Dulbecco's modified eagle medium (DMEM)	Corning	Cat#10-013-CV
Roswell Park Memorial Institute (RPMI) 1640 medium	Stemcell	Cat#36750
Fetal bovine serum (FBS)	VWR	Cat#89510-186
BSA	LGC Clinical Diagnostics	Cat#50-61-00
Paraformaldehyde Solution, 4% in PBS, Affymetrix/USB™	Fisher Scientific	Cat#AAJ19943K2
Penicillin/streptomycin	Corning	Cat#30-002-CI
Polyethylenimine (PEI) 25K MW, linear	Polysciences Inc	Cat#23966
Polyethylene glycol 8,000	VRC	Cat#JTU222-9
Puromycin	Sigma	Cat#P8833-10MG
DEAE-Dextran	Sigma	Cat#D9885-10G
Sodium Citrate	VWR	Cat#6132-04-3
Tris pH 8.00	Fisher Scientific	Cat#S1519-500GM
DNase I	NEB	Cat#M0303S
ATP	Sigma	Cat#A2383-5G
Magnesium chloride	BDH	Cat#BDH9244-500G
Magnesium sulfate	BDH	Cat#BDH9246-500G
Dithiothreitol (DTT)	VWR	Cat#97061-338
D-luciferin	Gold Bio	Cat#LUCK-2G
EDTA	Sigma	Cat#03690-100ML
Triton-X100	Fisher Scientific	Cat#BP151-500
Tween 20	Fisher Scientific	Cat#BP-337-100
Polybrene	Sigma	Cat#H9268-5G

(*Continued on next page*)

Continued

REAGENT or RESOURCE	SOURCE	IDENTIFIER
Gp120 protein for ELISA	Novus	Cat#NBP1-76371
Gp120 protein for ELISA (HIV_{JR-CSF})	Immune Technology	Cat#IT-001-0025p
Human recombinant IL-2	R&D Systems	Cat#202-IL-050
Critical Commercial Assays		
CD34 MicroBead Kit UltraPure, human	Miltenyi Biotec	Cat#130-100-453
HIV-1 p24ca antigen capture assay kit	Leidos Biomedical Research	https://frederick.cancer.gov/research/science-areas/aids-and-cancer-virus-program/cores/biological-products-core
TMB Microwell Peroxidase substrate system	SeraCare	Cat#50-76-00
QIAamp viral RNA mini kit	Qiagen	Cat#52906
Turbo DNase kit	Fisher Scientific	Cat#AM2239
PerfeCTa SYBR Green SuperMix, Low ROX	Quanta Biosciences	Cat#95056-500
qScript XLT 1-Step RT-qPCR ToughMix, Low-ROX	Quanta Biosciences	Cat#95134-500
SuperScript IV Reverse Transcriptase enzyme	ThermoFisher	Cat#18090050
Q5 Hot Start High-Fidelity DNA Polymerase	NEB	Cat#M0493L
Nextera XT Illumina library preparation kit	Illumina	Cat#FC-131-1096
D5000 ScreenTape System reagents	Agilent	Cat#5067-5589
MiSeq Reagent Kit v3	Illumina	Cat#MS-102-3003
MiSeq Reagent Kit v2	Illumina	Cat#MS-103-1003
KOD Hot Start Master mix	EMD Millipore	Cat#71975-3
Gel Purification Kit	Promega	Cat#A9282
In-Fusion HD cloning kit	Clontech	Cat#639650
EasySep™ Human $CD4^+$ T Cell Isolation Kit	STEMCELL Technologies	Cat#17952
QuickExtract DNA Extraction Solution	Biosearch Technologies	Cat#QE09050
Deposited Data		
HIV sequencing data	Short Read Archive (SRA)	SRA:PRJNA1399940
Experimental Models: Cell Lines		
HEK293T/17 Cells	ATCC	Cat#CRL-11268; RRID:CVCL_1926
TZM-bl	BEI Resources	Cat#ARP-8129; RRID:CVCL_B478
Experimental Models: Organisms/strains		
Female BLT-NOD-scid IL2Rg−/− (NSG) mice	Jackson Laboratory	Strain #005557; RRID:IMSR_JAX:005557
Oligonucleotides		
AAV qPCR primer 5′ AACGCCAATAGGGACTTTCC	Azenta Genewiz	N/A
AAV qPCR primer 3′ GGGCGTACTTGGCATATGAT	Azenta Genewiz	N/A
HIV qPCR Probe 56-FAM/CCCACCAAC/ ZEN/AGGCGGCCTTAACTG/3IABkFQ	Integrated DNA Technology	N/A
$HIV_{REJO.c}$ qPCR primer 5′ CAATGGCCCCAATTTCATCA	Azenta Genewiz	N/A
$HIV_{REJO.c}$ qPCR primer 3′ GAATGCCGAATTCCTGCTTGA	Azenta Genewiz	N/A
HIV_{JR-CSF} qPCR primer 5′ CAATGGCAGCAATTTCACCA	Azenta Genewiz	N/A
HIV_{JR-CSF} qPCR primer 3′ GAATGCCAAATTCCTGCTTGA	Azenta Genewiz	N/A
$HIV_{REJO.c}$ cDNA primer 3′ TTGGTACTTGTGATTGCTCCATGTCTCTCC	Azenta Genewiz	N/A

(*Continued on next page*)

Continued

REAGENT or RESOURCE	SOURCE	IDENTIFIER
HIV_{JR-CSF} cDNA primer 3′ CCCTATCTGTTGCTGGCTCAGCTCGTC	Azenta Genewiz	N/A
$HIV_{REJO.c}$ First round Nested PCR primer 5′ GCAATAGTAGCATTAGTAATAGCAGGAAT AATAGCAATAGTTGTGTGG	Azenta Genewiz	N/A
$HIV_{REJO.c}$ First round Nested PCR primer 3′ CTGCTCCCACCCCCTCTG	Azenta Genewiz	N/A
HIV_{JR-CSF} First round Nested PCR primer 5′ GCAATAATTGTGTGGTCCATAGTACTCATAGAA TATAGGA	Azenta Genewiz	N/A
HIV_{JR-CSF} First round Nested PCR primer 3′ CCCTATCTGTTGCTGGCTCAGCTCGTC	Azenta Genewiz	N/A
$HIV_{REJO.c}$ Second round Nested PCR primer 5′ AAAATAGACAGGTTAATTGATAGAATAAGAG ATAGAGCAGAAGACAGTG	Azenta Genewiz	N/A
$HIV_{REJO.c}$ Second round Nested PCR primer 3′ TCATTCTTTCCCTTACAGCAGGCCATC	Azenta Genewiz	N/A
HIV_{JR-CSF} Second round Nested PCR primer 5′ AAAATAGATAGGTTAATTGATAAAATAAGAG AGAGAGCAGAAGACAG	Azenta Genewiz	N/A
HIV_{JR-CSF} Second round Nested PCR primer 3′ TCATTCTTTCCCTTACAGTAGACCATCCAGGC	Azenta Genewiz	N/A
$HIV_{REJO.c}$ Env cloning primer 5′ GCAATAGTAGCATTAGTAATAGCAGGAATAA TAGCAATAGTTGTGTGG	Azenta Genewiz	N/A
$HIV_{REJO.c}$ Env cloning primer 3′ CTGCTCCCACCCCCTCTG	Azenta Genewiz	N/A
HIV_{JR-CSF} Env cloning primer 5′ GCAATAATTGTGTGGTCCATAGTACTCATAG AATATAGGA	Azenta Genewiz	N/A
HIV_{JR-CSF} Env cloning primer 3′ CCCTATCTGTTGCTGGCTCAGCTCGTC	Azenta Genewiz	N/A
Recombinant DNA		
ARP11746- WT – HIV-1, pREJO.c/2864 Strain IMC	BEI Resources	Cat#ARP-11746
ARP2708-WT – HIV-1, pYK-JRCSF Strain IMC	BEI Resources	Cat#ARP-2708
ARP11746- Env N160K (AAG)	This study	N/A
ARP11746- Env D167G (GGT)	This study	N/A
ARP11746- Env N276D (GAT)	This study	N/A
ARP11746 – Env T278K (AAG)	This study	N/A
ARP11746 – Env D279A (GCC)	This study	N/A
ARP11746 – Env A281D (GAT)	This study	N/A
ARP11746 – Env A281K (AAG)	This study	N/A
ARP11746 – Env N460D (GAT)	This study	N/A
ARP11746 – Env N276D (GAT) D279A (GCC)	This study	N/A
ARP11746 – Env N276D (GAT) A281D (GAT)	This study	N/A
ARP11746 – Env T278K (AAG) A281D (GAT)	This study	N/A
ARP11746 – Env D279A (GCC) N460D (GAT)	This study	N/A
ARP11746 – Env D loop from JR-CSF (RD)	This study	N/A
ARP11746 – Env V loop from JR-CSF (RV)	This study	N/A
ARP11746 – Env D and V loop from JR-CSF (RDV)	This study	N/A
ARP11746 – Env RV D279A (GCC)	This study	N/A
ARP11746 – Env RV D279H (CAC)	This study	N/A
ARP11746 – Env RV D279K (AAA)	This study	N/A

(*Continued on next page*)

Continued

REAGENT or RESOURCE	SOURCE	IDENTIFIER
ARP11746 – Pol M184I (ATA)	This study	N/A
ARP11746 – Pol M184V (GTG)	This study	N/A
ARP11746 – Pol M184V (GTG) Env N276D (GAT)	This study	N/A
ARP11746 – Pol M184V (GTG) Env D279A (GCC)	This study	N/A
ARP11746 – Pol M184V (GTG) Env N460D (GAT)	This study	N/A
ARP11746 – Pol M184V (GTG) Env N276D (GAT) D279A (GCC)	This study	N/A
ARP11746 – Pol M184V (GTG) Env D279A (GCC) N460D (GAT)	This study	N/A
ARP2708 – Env N160S (AGT)	This study	N/A
ARP2708 – Env N160Y (TAT)	This study	N/A
ARP2708 – Env N160K (AAA)	This study	N/A
ARP2708 – Env T162N (AAC)	This study	N/A
ARP2708 – Env T162P (CCC)	This study	N/A
ARP2708 – Env N276D (GAT)	This study	N/A
ARP2708 – Env D279A (GCC)	This study	N/A
ARP2708 – Env D279H (CAC)	This study	N/A
ARP2708 – Env D279N (AAC)	This study	N/A
ARP2708 – Env A281D (GAT)	This study	N/A
ARP2708 – Env N276D (GAT) A281D (GAT)	This study	N/A
AAV-VRC07 backbone plasmid	This study	N/A
AAV-N6 backbone plasmid	This study	N/A
AAV-PGDM1400 backbone plasmid	This study	N/A
AAV Helper plasmid (pHelp)	Balazs et al.[12]	https://doi.org/10.1038/nature10660
AAV Capsid plasmid (pAAV 2/8 Seed)	Balazs et al.[12]	https://doi.org/10.1038/nature10660
Software and Algorithms		
GraphPad Prism 10.2.2	Graphpad Software	www.graphpad.com/scientific-software/prism/; RRID:SCR_002798
Geneious Prime 2023	Geneious	http://www.geneious.com/; RRID:SCR_010519
FlowJo 10.9.0	FlowJo	https://www.flowjo.com; RRID:SCR_008520
Fluent Control	Tecan	https://lifesciences.tecan.com/fluent-laboratory-automation-workstation?p=tab–4
R v2023.06.1+524	Open-source software	https://cran.r-project.org/bin/windows/base/ RRID:SCR_001905
Python	Open-source software	http://www.python.org/ RRID: SCR_008394
Bowtie2	Open-source software	http://bowtie-bio.sourceforge.net/bowtie2/index.shtml RRID: SCR_016368
Fastp	Open-source software	https://github.com/OpenGene/fastp RRID: SCR_016962
samtools	Open-source software	http://htslib.org/ RRID: SCR_002105
snakemake	Open-source software	https://bitbucket.org/johanneskoester/snakemake/wiki/ RRID: SCR_003475
MonolixSuite 2023R1	Simulations Plus, Inc.	https://monolixsuite.slp-software.com/monolix/2024R1/
QuantStudio 12K Software v1.3	Applied Biosciences	https://www.thermofisher.com/us/en/home/global/forms/quantstudio-12k-flex-software-download.html
HIV sequencing data analysis pipeline	This study	https://doi.org/10.5281/zenodo.18187084

EXPERIMENTAL MODEL AND STUDY PARTICIPANT DETAILS

Human samples

All human samples were donated anonymously, with approval from the MGH Institutional Review Board, and informed consent was obtained from all tissue donors.

BLT Humanized Mice

BLT humanized mice were generated by the Human Immune System Mouse Program at the Ragon Institute of MGH, MIT, and Harvard. Briefly, 6- to 8-week-old female NSG mice were transplanted with human liver and thymus tissue under the kidney capsule and injected intravenously with 100,000 $CD34^+$ cells isolated from liver tissue by AutoMACS (Miltenyi Biotec, Cat#130-100-453). Mice were rested for 10 weeks after surgery to allow for recovery and engraftment. All experiments were approved by the Institutional Animal Care and Use Committee of the MGH and conducted in accordance with the guidelines and regulations of the American Association for the Accreditation of Laboratory Animal Care.

Cell Lines

Cell lines were obtained from ATCC and BEI resources and were not further authenticated. HEK293T/17 (ATCC, Cat#CRL-11268 - RRID:CVCL_1926) and TZM-bl (BEI Resources, Cat#ARP-8129 - RRID:CVCL_B478) cells originated from female donors. All cells were grown at 37°C, 5%CO_2, in DMEM medium (Corning, Cat# 10-013-CV) supplemented with 10% fetal bovine serum (FBS - VWR, Cat#89510-186), and 1% penicillin–streptomycin mix (Corning, Cat#30-002-CI).

METHOD DETAILS

HIV production

HIV was produced by transient transfection of HEK 293T/17 cells using 25K MW Linear Polyethyleneimine (PEI, Polysciences Inc., Cat#23966) maintained in DMEM medium supplemented with 10% and 1% penicillin–streptomycin mix with infectious molecular clone (IMC) plasmids encoding for $HIV_{REJO.c}$ or $HIV_{JR\text{-}CSF}$ (AIDS Reagent Program NIH - BEI Resources Cat#ARP-11746 and #ARP-2708, respectively) or IMC plasmids containing the indicated mutations. After 48 hours, culture supernatants were collected, filtered through a 0.45-m filter, and titered using either an HIV-1 p24 antigen capture assay (AIDS and Cancer Virus Program, Leidos Biomedical Research, Inc., Frederick National Laboratory for Cancer Research) or a 50% tissue culture infective dose ($TCID_{50}$) assay on TZM-bl cells. $TCID_{50}$ was calculated using the Spearman-Karber formula.[103]

Humanized mouse HIV infection

Prior to HIV infection, blood samples were obtained from mice and subjected to flow cytometry to determine the baseline $CD3^+$ (BioLegend, Cat#300434 - RRID:AB_10962690), $CD4^+$ (BioLegend, Cat#300534 - RRID: AB_2563791), and $CD8^+$ (BioLegend, Cat#300554 - RRID: AB_2564382) T cells engraftment. The next day, mice were intravenously infected with either 10ng of p24 or 300 $TCID_{50}$ of $HIV_{REJO.c}$ or $HIV_{JR\text{-}CSF}$ diluted in PBS (Corning, Cat#21-031-CV) to a volume of 50 μL. Blood was collected weekly to determine viral loads and bNAb concentration in serum.

AAVs vector production, quantification, validation, and administration

AAV8 vectors encoding either Luciferase, 2A10, or bNAbs were produced and validated as previously described.[12] Briefly, HEK293T/17 cells were co-transfected with the AAV backbone vector and helper vectors pHELP and pAAV 2/8 SEED using PEI. AAVs were collected over a five-day period following transfection, filtered through a 0.22 μm filter (Corning, Cat#431097), and fresh media was gently added back to the cells each time. After collection, the virus was Polyethylene glycol 8,000 (PEG, VWR, Cat#JTU222-9) precipitated on ice O.N., and then pelleted at 8,000 x g for 30 min. Pellets were re-suspended in cesium chloride, split evenly into two Quick-Seal tubes (Beckman, Cat#342413) and centrifuged at 330,000 x g at 20 °C for 24 h (Beckman Coulter, Optima LE-80K, 70Ti rotor). AAV-containing fractions were determined with a refractometer, with refractive indexes between 1.3755 and 1.3655 considered positive. These were then diluted into 15l mL of Test Formulation Buffer 2 (TFB2, 100 mM sodium citrate (VWR, Cat#Cat#6132-04-3), 10 mM Tris, pH 8.00 (Fisher Scientific, Cat#S1519-500GM)), loaded in a 100 kDa MWCO centrifugal filter (Millipore, Cat#UFC910024) and centrifuged at 500 x g at 4 °C until 1 mL remained in the filter. This wash was repeated twice. Final retentate was aliquoted and stored at −80 °C. Purified AAVs were quantified by qPCR using the PerfeCTa SYBR Green SuperMix, Low ROX (Quanta Biosciences, Cat#95056-500) and primers designed against the CMV enhancer (AACGCCAATAGGGACTTTCC and GGGCGTACTTGGCATATGAT). Samples were run in duplicate on an QuantStudio 12K Flex (Applied Biosystems). To validate the functional activity of each lot, *in vitro* transduction assays were performed in HEK293T/17 cells. Six days after transduction, supernatants were recovered and quantified for total IgG production by ELISA. AAV8 IM injections were performed as previously described.[12] Briefly, aliquots of previously titered viruses were thawed on ice and diluted in PBS to achieve the predetermined dose in a 40 μL volume. A single 40 μL injection was administered into the gastrocnemius muscle of BLT humanized mice with a 28 G insulin syringe.

Antibody quantification by ELISA

Plasma was used to determine bNAb concentrations. For detection of gp120-binding IgG, ELISA plates were coated with 2 μg/mL of HIV gp120 protein (Novus, Cat#NBP1-76371 or Immune Technology, Cat#IT-001-0025p) per well for 1h at room temperature. For detection of PGDM1400, ELISA plates were coated with BG505 SOSIP (provided by the Vaccine Research Center) at 5 μg/mL or a PGDM1400-specific idiotype (provided by Dan Barouch) at 1 μg/mL for 2hr at room temperature. Plates were blocked with 1% BSA (LGC Clinical Diagnostics, Cat#50-61-00) in Tris-buffered saline (TBS - Thermo Scientific, Cat#AAJ75892AE) overnight at 4°C. Samples were incubated in TBS plus Tween 20 (Thermo Scientific, Cat#BP-337-100) containing 1% BSA for 1h at room temperature before incubation with 1:2,500 to 1:10,000-diluted horseradish peroxidase (HRP)-conjugated goat anti-human IgG-Fc antibody (Bethyl, Cat#A80-104A - RRID: AB_67064) for 30 min at room temperature. Samples were detected by the TMB Microwell Peroxidase substrate system (SeraCare, Cat#50-76-00). A standard curve was generated using purified VRC07, N6, or PGDM1400 (provided by the Vaccine Research Center) as appropriate for the sample.

Viral load test by quantitative RT-PCR (RT-qPCR)

Viral RNA was extracted from plasma samples using the QIAamp viral RNA mini kit (Qiagen, Cat#52906)). Each RNA sample was treated with 2 U of Turbo DNase (Fischer Scientific, Cat#AM2239) at 37°C for 30 min followed by heat inactivation at 75°C for 15 min. 10 μL of the treated RNA were used in a 20 μL RT-qPCR reaction with the qScript XLT one-step RT-qPCR Tough Mix, low ROX mix (Quanta Biosciences, Cat#95134-500), a TaqMan probe (5'-/56-FAM/CCCACCAAC/ZEN/AGGCGGCCT-TAACTG/3IABkFQ/-3') (IDT) and primers designed targeting the Pol gene of $HIV_{REJO.c}$ (CAATGGCCCCAATTTCATCA and GAATGCCGAATTCCTGCTTGA) or HIV_{JR-CSF} (CAATGGCAGCAATTTCACCA and GAATGCCAAATTCCTGCTTGA). Samples were run in triplicate on a QuantStudio 12K Flex (Applied Biosystems). The following cycling conditions were used: 50°C for 10 min, 95°C for 3 min followed by 55 cycles of 95°C for 3s and 60°C for 30s. Virus titer was determined by comparison with a standard curve generated using RNA extracted from serially diluted mixture of commercially titered viral stock and pure mouse serum. The limits of detection were 1,000 copies per mL for all viral strains. For the purpose of generating Kaplan-Meier curves, viral escape was defined as the earliest week after AAV administration in which viral load did not decrease by at least 75% relative to the prior week and remained above 10^4 copies per mL, provided that a subsequent week was also above that threshold. Curves were analyzed for statistical significance using the Mantel-Cox Log-rank test in Graphpad Prism v10.2.2 (RRID:SCR_002798).

Illumina deep sequencing and identification of HIV envelope mutants

Viral RNA extracted from blood samples at the conclusion of each study was used to synthesize cDNA using the SuperScript IV Reverse Transcriptase enzyme with a strain-specific 3' primer for $HIV_{REJO.c}$ (TTGGTACTTGTGATTGCTCCATGTCTCTCC) or HIV_{JR-CSF} (CCCTATCTGTTGCTGGCTCAGCTCGTC). cDNA was subjected to nested PCR amplification with HIV-specific envelope primers that yielded a 2.5-kb fragment. The initial round primers used for amplification from $HIV_{REJO.c}$ were GCAATAGTAGCATTAGTAATAGCAGGAATAATAGCAATAGTTGTGTGG and CTGCTCCCACCCCCTCTG; whereas the primers used for envelope amplification from HIV_{JR-CSF} were GCAATAATTGTGTGGTCCATAGTACTCATAGAATATAGGA and CCCTATCTGTTGCTGGCTCAGCTCGTC. First-round PCR was performed with 1 to 2.5 μL from cDNA reaction using 1x Q5 reaction buffer, 5 mM dNTPs, 0.5 μM of strain specific primers and 0.02U/μL of Q5 Hot Start High-Fidelity DNA Polymerase (NEB, Cat#M0493L) in a total reaction volume of 25 μL. PCR conditions for initial round were: 98°C for 30s, followed by 30 cycles of 98°C for 10s, 70°C for 30s, 72°C for 3 min, with a final extension of 72°C for 2 min. 1μL of first round PCR product was then used as the template for the second round PCR with identical cycling conditions and PCR mix except for the primers. The second-round primers used for envelope amplification from $HIV_{REJO.c}$ were AAAATAGACAGGTTAATTGATAGAATAAGAGATAGAGCAGAAGACA-GTG and TCATTCTTTCCCTTACAGCAGGCCATC; whereas the primers used for envelope amplification from HIV_{JR-CSF} were AAAATAGATAGGTTAATTGATAAAATAAG- AGAGAGAGCAGAAGACAG and TCATTCTTTCCCTTACAGTAGACCATCCAGGC. PCR products were gel extracted, diluted to 0.15 ng/μL in UV-irradiated water and subjected to Nextera XT Illumina library preparation (Illumina, Cat#FC-131-1096). PCR products were quantified using Qubit and D5000 ScreenTape System (Agilent, Cat#5067-5589). The library pool was denatured with 0.2 N NaOH, diluted to 4 nM, spiked with 10% PhiX to improve sequence heterogeneity and quality and subjected to 2 x 250 or 2 x 300 paired-end sequencing on the Illumina MiSeq (RRID:SCR_016379).

Envelope Escape Mutant Analysis

Sequencing reads were filtered for quality using fastp (RRID: SCR_016962)[104] and aligned to a reference sequence specific to the viral strain under analysis using Bowtie2 (RRID: SCR_016368).[105] The alignments were sorted and indexed using samtools (RRID: SCR_002105).[106] Amino acid changes were called using a custom codon aware variant caller, written in python (RRID: SCR_008394). For each sample, the total divergence at each amino acid site was determined by summing the frequency of every non-WT amino acid (relative to the IMC strain sequence, meaning that synonymous mutations are not considered divergent). The group amino acid divergence (plotted in the figures) was determined by averaging the amino acid divergence across each sample at every site. Each site was numbered using the HIV_{HXB2} nomenclature.[107] The analysis pipeline was run using snakemake (RRID: SCR_003475).[108] All the bioinformatics tools used in these analyses are available online at https://github.com/Balazs-Lab/Escapability.

Viral Diversity and Variant Conservation Analysis

Similar to the envelope escape mutation analysis, sequencing reads were filtered for quality using fastp[104] and aligned to a reference sequence specific to the viral strain under analysis using Bowtie2.[105] The alignments were sorted and indexed using samtools.[106] SNVs were called using LoFreq.[109] The heterogeneity of each sample was determined using the SNV data to calculate the average Shannon entropy across all sites in the viral envelope, as performed previously.[110,111] The Shannon entropy at each site in the genome was calculated by taking the sum of the frequency of each SNV times the natural log of the SNV frequency (frequency * ln(frequency)), multiplied by negative one. The analysis pipeline was run using snakemake[108] and is available online at https://github.com/Balazs-Lab/Escapability. For the comparison of viral diversification to the LANL database, the HIV1 FLT 2022 Env Protein Alignment was downloaded from LANL and filtered for subtype B sequences. All positions were numbered based on their HIV_{HXB2} alignment and only positions shared across $HIV_{REJO.c}$, HIV_{JR-CSF}, and the LANL database were analyzed. The average frequency of each $HIV_{REJO.c}$ and HIV_{JR-CSF} amino acid was binned by rounding the log_{10} transformed frequency using the MROUND() function in excel. These grouped bins were then used to evaluate the LANL amino acid frequency data, of which the average and standard deviation were calculated using the Excel Pivot Table functions.

Construction of HIV mutants

Individual mutations were introduced into the parental IMC vectors expressing the molecular clone using overlapping PCR with primers incorporating the desired mutations. After amplification of the *env* or *pol* gene with the mutagenesis primers using KOD Hot Start Master mix (EMD Millipore, Cat#71975-3) or Q5 Hot Start Master Mix (NEB, Cat#M0493L), the PCR product was purified by gel extraction (Promega, Cat#A9282) and cloned by homologous recombination into the appropriate recipient parental backbone vector using the In-Fusion HD cloning kit (Clontech, Cat#639650). The ligation product was transformed into DH5α (Zymo, Cat#T3009) or SURE2 (Agilent, Cat#200152) competent cells, and positive clones were full plasmid sequenced.

In vitro neutralization assay

To compare the sensitivity of point-mutant viruses to bNAb antibody neutralization, each mutant was produced by transient transfection of HEK 293T cells as described above and viral supernatants were titered by $TCID_{50}$ on TZM-bl cells. Then, neutralization assays were performed using a TECAN Fluent 780 liquid handler by mixing 20 μL of virus with 20 μL of 2.5-fold serial dilutions of each antibody and incubating this mixture at 25°C for 1 h. After the incubation, antibody-virus mixtures were added to previously plated 6,000 TZM-bl cells with 75 μg per mL of DEAE dextran (Sigma, Cat#D9885-10G) and incubated at 37°C for 48 h. Cells were then lysed using luciferin-containing buffer[112] and Luciferase signal was quantified using a PHERAstar FSX plate reader (BMG LabTech). Percentage of infection was determined by calculating the difference in luminescence between test wells (cells with virus and antibody) and cell control wells (cells only) and dividing this value by the difference between the virus control wells (cells with virus) and the cell control wells. These values were plotted against antibody concentrations and fitted into a four-parameter nonlinear regression to calculate IC_{50} and Hill Slope using GraphPad Prism v10.2.2.

Determination of viral fitness

In silico viral growth curves were generated with growth rates derived from *in vitro* QuickFit assays as described previously.[65] Briefly, commercially acquired human PBMCs (AllCells, Cat#PB004F; Lot #A2857) were thawed and $CD4^+$ T cells were isolated using the EasySep™ Human $CD4^+$ T Cell Isolation Kit (STEMCELL Technologies, Cat#17952). Naive $CD4^+$ T cells were resuspended in complete RPMI 1640 (Corning, Cat#36750) (cRPMI; 10% FBS and 1% penicillin/streptomycin) supplemented with 10 ng/mL recombinant IL-2 (R&D Systems, Cat#202-IL-050) and 4 μg/mL of anti-CD28 antibody (Biolegend, Cat#302934 - RRID: AB_11148949), plated in 24-well plates coated with 2 μg/mL of anti-CD3 antibody (Biolegend, Cat#317326 - RRID: AB_11150592), and incubated at 37°C and 5% CO_2 for 4 days. Cells were then pooled and incubated for another 4 days before use. Purification and activation efficiency were evaluated by flow cytometry. Previously titered viruses were three-fold serially diluted and then added to 50 μL of activated $CD4^+$ ($1x10^5$ cells per well) plated in a 96 round-well plate. Viruses and cells were spinoculated at 1,200 RPM for 1 hour at 20°C, and then incubated for 24 hours at 37°C with 5% CO_2. Cells were washed five times with 200μL of cRPMI, resuspended in 200 μL of fresh cRPMI plus 10 ng/mL of IL-2 and finally transferred to a 96 flat-well plate. Plates were incubated at 37°C with 5% CO_2 for 6 days. 32 μL of supernatant were collected daily and fresh media was added to replace the volume. Collected supernatants were immediately RNA extracted using QuickExtract DNA Extraction Solution (Biosearch Technologies, Cat#QE09050).[65] Extracted RNA was used to determine viral loads by RT-qPCR as stated above. Viral loads were used to determine growth rates and generate *in silico* growth curves using a half-maximal equation in MonolixSuite 2023R1 (Lixoft).

Escape Barrier Analysis

Sample specific sequencing data from the Envelope Escape Mutant Analysis was used to generate sample specific escape haplotypes. Sequences from each escaped sample were filtered for a minimum mutation frequency of at least 10%, and then manually classified into an escape path using the decision tree algorithms described in Figures S3 and S8. The area under the curve (AUC) for each escape path was calculated from the IC_{50} values and relative fitness cost data using the trapz function in the pracma[113] package in R (RRID:SCR_001905).[114] The calculation began at the WT coordinate for each virus and summed the AUC up to the position of the escaped haplotype. If the escape IC_{50} was greater than 200 μg/mL (the limit of detection), then the X-coordinate for IC_{50} was assigned a value of 200 μg/mL, otherwise the IC_{50} of the escape haplotype was used. For all samples (except the HIV_{RV} escape)

only escape paths A and B were used for the Escape Barrier score analysis because they represented at least 50% of the escape paths. The raw AUC value for each path was scaled by the relative proportions of the paths (Relative Fraction value in Figures S4D and S8E). The path scaled AUC scores were then summed to create the Escape Barrier Score. The scripts and coordinate files are available at https://github.com/Balazs-Lab/Escapability.

Passive transfer experiments

Humanized BLT mice were infected with HIV_{JR-CSF} as described above, and 4 weeks later were passively infused with 25 μg per gram of body weight of a control antibody (2A10), N6 or PGDM1400, weekly for 12 weeks. Blood was collected weekly to determine viral loads and bNAb concentration in serum.

In vivo antiretroviral selection-pressure of HIV

To select for ART-escaping HIV mutations, individual tablets of emtricitabine (Emtriva™ (FTC), Gilead Sciences) or Tenvir (tenofovir disoproxil fumarate (TDF); Cipla LTD) were crushed into a fine powder and manufactured with TestDiet 5B1Q feed (Modified LabDiet 5058 with 0.12% amoxicillin) into powder. The final concentration of these drugs in the stock food was 2.3% (4500 mg/kg TDF, 3000 mg/kg FTC).[28] To achieve a comparable human dose (i.e., 200 mg FTC, 300 mg TDF), the Reagan-Shaw formula[115] was used to translate the dose from human to mouse with the assumption that an average mouse weighs 20 g and a human weighs 60 kg. On average mice ate 2 g of food per day and the powdered ART-food was diluted in normal TestDiet 5B1Q food to achieve ingestion of the corresponding target human dose per day. BLT mice were infected with $HIV_{REJO.c}$ as previously stated and over the course of 6 weeks, we titrated the dose of ART drug in their food, from 1% to 100% of the standard human equivalent dose (1% for weeks 2 and 3, 10% for weeks 4 through 6, 100% until week 10). At week 8, mice were injected with AAV expressing VRC07 or Luciferase as stated above. At week 10, ART treatment was interrupted. Blood samples were collected weekly to evaluate viral loads and antibody expression.